I.

NeuroReport 10, 2539–2545 (1999)

Calcium-containing endosomes at oculomotor terminals in animal models of ALS

László Siklós,[1,2] József I. Engelhardt,[1,3] Róbert Adalbert,[2] and Stanley H. Appel[1,CA]

[1]Department of Neurology, Baylor College of Medicine, One Baylor Plaza, Houston, TX 77030, USA; [2]Institute of Biophysics, Biological Research Center, Szeged; [3]Department of Neurology, Albert Szent-Györgyi School of Medicine, Szeged, Hungary

[CA]Corresponding Author

ALTERED calcium homeostasis has been demonstrated in human spinal cord motor axon terminals of ALS patients, in spinal motor neurons of mutant SOD transgenic mice and following injection of ALS immunoglobulins. In all three paradigms oculomotor neurons are relatively spared. To explore mechanisms of selective resistance, we applied similar calcium localization techniques to terminals of oculomotor neurons in the two animal models. In both cases large vacuoles, which connect with the extracellular space, accumulated the majority of intracellular calcium, while terminals of vulnerable neurons (e.g. innervating interosseus muscle), which possess no such vacuoles, displayed evenly distributed calcium. These relatively unique membrane enveloped structures may permit neurons to control their cytoplasmic Ca^{2+} concentration and contribute to selective resistance. *NeuroReport* 10:2539–2545 © 1999 Lippincott Williams & Wilkins.

Key words: ALS; Animal models; Calcium; Degeneration; Endosome; Motoneuron; Resistance; Vulnerability

Introduction

Impairment of neuronal calcium homeostasis is one of the major mechanisms converting initial injury to irreversible destruction [1]. However, the specific mechanisms, which make particular neuron populations vulnerable or resistant to a large calcium load are undefined, although the relative presence or absence of calcium binding proteins may play a role. The availability of animal models of neurodegenerative diseases provide a unique opportunity for study with the slow development of clinical signs and pathological alterations and the possibility that corresponding changes in intracellular calcium may also follow a similarly slow time course. Thus, on a time scale of several weeks suitable images can be obtained with conventional ultrastructural methods to characterize intracellular calcium distribution in neurons with different vulnerability.

For this study, animal models of familial and sporadic forms of the lethal motoneuron disease amyotrophic lateral sclerosis (ALS) were selected because disturbed calcium homeostasis in ALS has already been documented. In our previous studies we detected increased calcium accumulation in motor nerve terminals of sporadic ALS patients [2]. Similar changes could be transferred to experimental mice with immunoglobulin (IgG) preparations from sporadic ALS patients [3]. Additionally, modification of the calcium distribution within spinal motoneurons was noted in a transgenic mouse model of one of the forms of familial ALS [4], based on a $G^{93}\rightarrow A$ mutation of the gene encoding Cu/Zn superoxide dismutase (SOD1) [5]. However, a surviving population of motoneurons, those of the oculomotor nucleus [5], were relatively spared even though they possessed the same genetic defect. In the present study we demonstrate that this viable group of neurons possesses special morphological features, which might affect their calcium homeostasis, thus contribute to selective resistance in models of familial and sporadic ALS.

Materials and Methods

Transgenic animals: SOD1 mutant (G1H/+) and wild type (N29/+) mice were obtained from Jackson Laboratory (Bar Harbor, Maine). The G1H/+ line contains the entire human SOD1 gene expressing the $G^{93}\rightarrow A$ mutation; the N29/+ line contains the wild-type human SOD1 gene and expresses levels of human Cu/Zn SOD protein comparable with the level of mutant Cu/Zn SOD protein in G1H/+ mice [4]. The presence of endosomes was checked in nerve terminals at 2, 3, 4 and 5 months of age in one pair of N29/+ and G1H/+ animals per time point;

12–18 endplates were examined from the interosseus- and external eye muscles (regularly the superior rectus) of each animal.

Passive transfer model: Rats were injected i.p. every day for 30 days with IgG from a patient with sporadic ALS or a patient with chronic inflammatory demyelinating polyneuropathy (CIDP), who served as a control. To reduce immune response against foreign IgG neonatal rats were selected for injection. The treatment started on the day of birth with a low dose injection (10 mg protein), which was increased gradually to 20 mg protein in 10 days. Pups (two in each group) were then injected with 20 mg protein daily until they were killed at the age of 1 month. Similar muscles were examined as in case of SOD1 transgenic animals; 10–15 endplates were collected for microscopy from each muscle.

Calcium cytochemistry: Animals were transcardially perfused under ketamine anesthesia with 3% glutaraldehyde containing 90 mM oxalic acid. Tissue samples were removed, fixed for additional 12 h in the same fixative followed by postfixation in 1% osmic acid containing 1% K-pyroantimonate, then dehydrated and embedded in plastic [5]. Ultrathin sections were cut which were used both for analytical control of the reaction product and ultrastructural description of the tissue. The procedure preserved the ultrastructure of the tissue and yielded electron dense deposits at places where oxalic anions trapped tissue calcium.

Analytical microscopy: Unstained, 30–40 nm thin sections were cut for electron spectroscopic imaging to prove the calcium content of the reaction product of the histochemical procedure. Sections were screened at the carbon absorption edge (dE = 250 eV energy loss value) to select tissue features for analytical microscopy. Analysis was performed by recording image pairs above (dE = 350 eV) and below (dE = 315 eV) the calcium edge, then images were subtracted to produce two-dimensional distribution of calcium at the selected field of view. This image was then contrast enhanced and color-coded according to the significance of the signal at each image point, then superimposed onto the corresponding structural image to prove the correlation of the true calcium signal with the distribution of electron dense deposits visible in conventional electron microscopy. Electron spectroscopic imaging was performed in a Zeiss CEM 902 electron filtering microscope.

Results

The most striking feature of oculomotor nerve terminals from both SOD1 transgenic mice and rats injected with ALS IgG was the appearance of large (2–3 μm) intracellular vacuolar structures (endosomes; Fig. 1a–d). These structures were not seen in the same animals in nerve terminals innervating interosseus muscle (representing a vulnerable cell type), or in oculomotor terminals of wild type control mutant mice or rats injected with non-ALS IgG. Thus, they may represent a unique response of a resistant motoneuron cell type to the applied 'ALS-like' stress conditions. With the calcium precipitation technique large clusters of electron dense calcium containing precipitates were present in the lumen of these vacuoles, while neighboring mitochondria and cytoplasm were practically devoid of deposits (Fig. 1a–d). This finding was in contrast to terminals of vulnerable neurons, where mitochondria loaded with calcium were observed (Fig. 2a–d). Since these findings suggested that the endosomes might function as a calcium sink, we examined a series of consecutive sections cut from oculomotor terminals from SOD1 transgenic and ALS IgG-injected animals to determine the contiguity of the vacuolar membrane with other structures. This analysis revealed that the vacuoles in both models could establish direct spatial connections with the extracellular space (Fig. 1e,f). Such connections were difficult to find and were usually observed in a single section only, suggesting that they were actually confined to a very narrow area. It is also feasible that some of the endosomes did not possess such a communication channel at the time of fixation.

To determine intracellular calcium distribution in motor nerve terminals, deeply anesthetized animals were perfused transcardially according to the oxalate–pyroantimonate method to trap and fix tissue calcium, and processed for electron microscopy. The procedure resulted in finely dispersed electron dense precipitates over the cytoplasm with occasional clusters mainly in membrane enclosed organelles. Although the procedure is inferior to quick freezing methods, when conservation of total and *in situ* elemental distribution is paramount [6], the precipitation technique is still useful for comparison to suitably selected controls. Unlike freezing methods, this technique provides excellent ultrastructural preservation of the entire volume of the sample and does not introduce structural alterations compared to the ultrastructural standard of conventional perfusion fixation [7]. Throughout the study the analytical specificity of the method was regularly controlled (Fig. 3a–e).

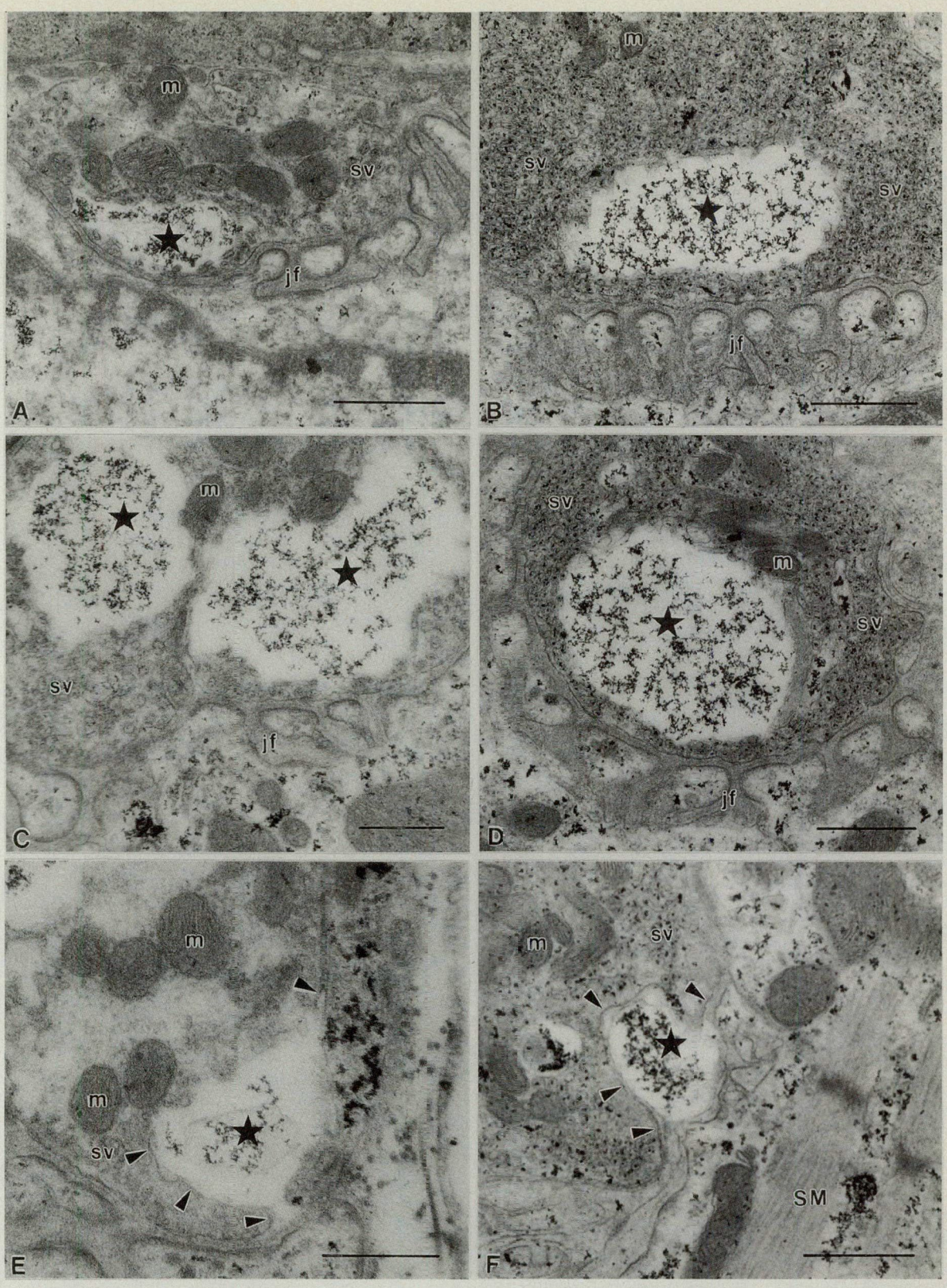

FIG. 1. Ultrastructure of oculomotor nerve terminals from SOD1 mutant mice (**A**,**C**,**E**) and from rats injected with ALS IgG (**B**,**D**,**F**). Large calcium accumulating vacuolar structures can be seen in each figure (star), while mitochondria and cytoplasm are practically devoid of black precipitates corresponding to the distribution of tissue calcium content. In both species spatial connection of the large vacuoles with the extracellular space could be demonstrated (E,F). Such connections were, however, difficult to find, implying that they were restricted to a narrow area. It is also possible that some of the endosomes did not possess such a communication channel at the time of fixation. Characteristically, synaptic vesicles may also contain calcium. m: mitochondrion, sv: synaptic vesicles, jf: junctional folds (specialized postsynaptic membrane), SM striated muscle; arrowheads point to nerve terminal membrane segments outlining vacuoles proving that their content can flow in or out to the extracellular space depending on the electrochemical gradient of their constituents. Bar = 0.5 μm.

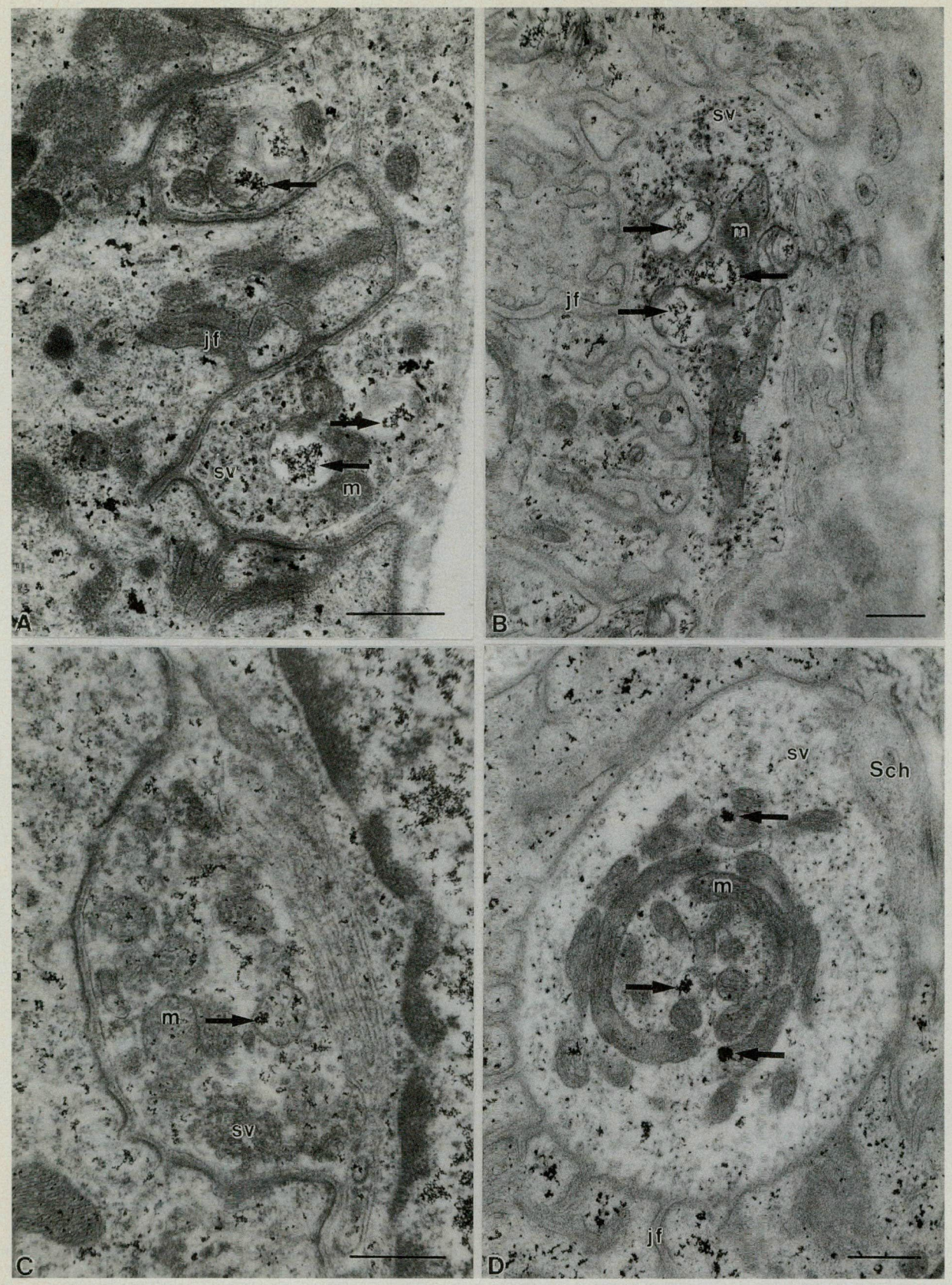

FIG. 2. Motor nerve terminals from the interosseus muscle, a prototype of vulnerable nerve terminals in ALS, from SOD1 mutant mouse (**A**,**C**) and from a rat injected with ALS IgG (**B**,**D**). No vacuoles can be seen, while mitochondria are loaded with calcium with different degree. To illustrate the variability of mitochondrial calcium precipitation, (A) and (B) display mitochondria with large amounts of electron dense precipitates disrupting mitochondrial structure, while (C) and (D) display a situation with lighter precipitates when the mitochondrial structure is still intact. m: mitochondrion, jf: junctional folds, sv: synaptic vesicles, Sch: Schwann cell envelope. Bar = 0.5 μm.

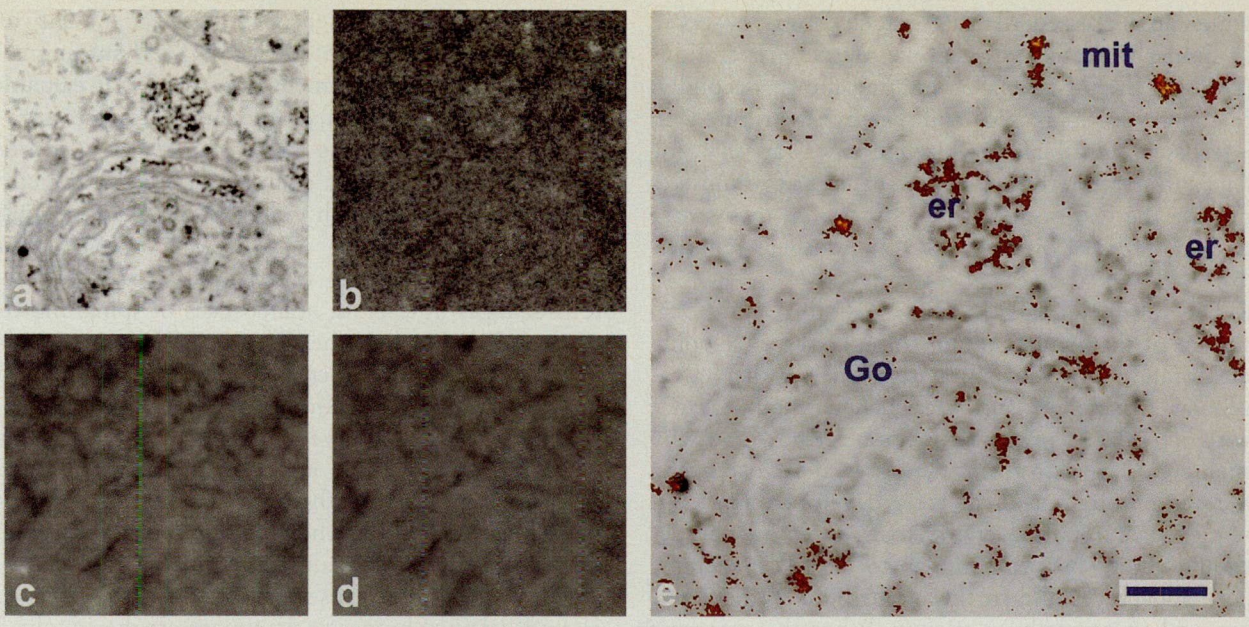

FIG. 3. Spinal motoneurons from SOD1 mutant transgenic mice with a usual feature of heavy calcium precipitates in mitochondria, Golgi apparatus and endoplasmic reticulum. (**a–d**) The steps of analytical proof of calcium content of the reaction product of the oxalate–pyroantimonate fixation procedure. (a) Structural imaging of unstained section at the carbon absorption edge (dE = 250 eV) yields high contrast micrograph after inverting a dark field-like original image. (c,d) Imaging above and below the calcium absorption edge gives low contrast pictures containing basic analytical information for calcium distribution. The difference image of (c) and (d) is shown in (b), which is the net calcium distribution of the same field, superimposed on the background noise. This image is used to calculate the background level and background noise (mean, s.d.) to determine the final net calcium distribution. Calcium level at each image point was accepted to be significant if it was above the background level with at least 2× s.d. According to the actual significance level at each pixel the true calcium distribution was color coded and superimposed onto the corresponding structural image in (**e**). Go: Golgi apparatus, er: endoplasmic reticulum, mit: mitochondrion. Bar = 0.2 μm.

Discussion

The origin or identity of the intracellular vacuoles (endosomes) could not be determined on the basis of these experiments, although a number of membrane enclosed organelles such as mitochondria [8], smooth endoplasmic reticulum (SER) [9], calciosomes [10] and caveolae [11] are known to participate in intracellular calcium regulation. On the basis of ultrastructural appearance, mitochondria could be excluded, but less is known about the structure of the remaining three candidates. They are all equipped with essential components for regulation of intracellular calcium, i.e. Ca^{2+} pump ATPase and IP_3-receptor/Ca^{2+} channel for regulation of transmembrane ion fluxes. SER and calciosomes are also equipped with calreticulin, a high-capacity calcium binding protein [12]. However, none of these structures share the morphological features of vacuoles of the present study. SER and calciosomes would not be expected to connect with the extracellular space. Caveolae do communicate with the extracellular space, and possess calcium sequestering capacity and a role in regulation of intracellular calcium homeostasis. However, their characteristic size is in the range of 100 nm, which is orders of magnitudes smaller than the described vacuoles. Thus, the observed calcium containing endosomes could be either known organelles with novel features, or newly formed structures. Nevertheless, studies of vesicle recycling do suggest a mechanism for endosome formation.

Stimulation of nerve terminals has been reported to lead to a transient increase of endosome-like organelles, because of the different kinetics of exo- and endocytosis [13]. Further, the removal of extracellular calcium can lead to persistent formation of vacuole-like structures by uncoupling vesicle exocytosis and endocytosis [14]. These vacuoles could possess very narrow channels communicating with the extracellular space [14], similar to the endosomes documented in our study. The endosomes described by Takei and co-workers [13] retained extracellular markers, suggesting that they could actually pinch off, and be functionally characterized as intracellular organelles [13]. Increased intracellular calcium has been demonstrated to hinder vesicle membrane retrieval in a graded fashion [15,16]. Thus, differential formation of endosomes in vulnerable and resistant motoneurons could result from different ways of handling intracellular calcium possibly influenced by calcium binding protein content. Differential calcium homeostasis in such neurons is supported by two earlier observations. First, ALS IgG increased miniature end-plate potential (MEPP) frequency in the extensor digitorum longus muscle,

while no increased MEPP frequency was observed in similarly treated external eye muscle preparations (D.R. Mosier, personal communication). Secondly, calcium was increased and evenly distributed in interosseus terminals [3,5], while it was at very low levels in nerve terminals of the external eye muscles outside the endosomes, and only started to increase at later stages of disease in SOD1 transgenic animals [5].

The ultimate identification requires additional studies of the protein composition of the enveloping membranes, their structural relation to other intracellular organelles, and the change in appearance with activity. At present it is not clear how and why such endosomes do form. However, if endosomes in the oculomotor terminals were developed as a consequence of retarded endocytosis, their membranes should likely be very similar to the plasmalemma [13], and they could further contribute to the active removal of intracellular calcium. When the capacities of the calcium homeostatic mechanisms are finally overwhelmed (either due to chronic ALS IgG injections or to late in the course of mutant SOD1 disease), the overall intraterminal calcium could also be increased in oculomotor axon terminals, with a parallel disappearance of endosomes, as documented in SOD1 transgenic animals [5].

Regardless of the specific identity of the described vacuoles, their observed calcium sequestering capability and extruding potential have direct implications for our present knowledge of the pathomechanism of ALS. Thus, mutations in SOD may contribute to impaired free radical homeostasis, which may, in turn, impair calcium homeostasis implying that oxidative stress can cause calcium stress *in vivo*. Although direct evidence for free radical production has not been demonstrated, nor can altering wild type SOD in the presence of SOD mutation rescue motoneurons [17], neuronal vulnerability still appears to depend on calcium entry and deficiency in cytosolic calcium binding proteins [18]. As a consequence, elevated calcium content could be documented in vulnerable spinal motoneurons (Fig. 3). Although no such increase could be observed in the cell bodies of oculomotor neurons [5], evidence of altered calcium homeostasis is present in the nerve terminals and unique structures could relieve the cell of the high calcium load (Fig. 2a–f).

Our data suggest that elevated intracellular calcium may be the common pathway leading to the clinically identical manifestations of sporadic and familial ALS. SOD1 mutations are noted only in familial ALS but not in sporadic ALS [19]. Thus, free radical stress may be only one of several potential triggers leading to increased calcium. Indeed, both of the extensively studied models of sporadic ALS, i.e. excitotoxicity [20] and autoimmunity [21], imply involvement of intracellular calcium in the pathomechanism of the disease, since intracellular calcium can be raised either as a consequence of glutamatergic overstimulation, or directly by calcium flux through voltage-dependent calcium channels enhanced by ALS IgG [22]. ALS IgG passively transferred to mice could induce deleterious changes in calcium homeostasis of spinal motoneurons [3]. Further, the $G^{93}\rightarrow A$ SOD mutation is also associated with increased intracellular calcium in motoneurons [5]. Since a common defense response could be observed in oculomotor terminals of SOD1 mutant mice, and rats injected with ALS IgG, we suggest that the triggering insult for this mechanism might be the same in both cases, i.e. increased intracellular calcium.

While the initial causes of ALS may be diverse, altered calcium homeostasis appears to be involved in the final common pathway of motor neuron injury and cell death. In human ALS biopsies, we detected a failure of calcium homeostasis in affected cells with selective calcium accumulation in motor nerve terminal of patients with sporadic ALS [2]. We have described preferential enrichment of certain calcium binding proteins in motoneuron populations, which are relatively resistant to the disease, in both human material [23] and in SOD mutant transgenic animals [5]. Now we report novel ultrastructural features of a population of surviving motoneurons, which may represent the morphological manifestations of a mechanism to maintain cytoplasmic calcium level in the physiological range. It is possible that the presence of parvalbumin in oculomotor neurons may contribute to the development of these unique structures. Understanding the details of processes underlying the formation of the observed calcium sequestering vacuolar structures may provide insight into the defense mechanisms of resistant neurons against calcium-mediated stress and might provide clues to design successful rescue strategies for the vulnerable population.

Conclusion

We demonstrated that nerve terminals of those motoneurons, which are typically resistant in ALS, could develop unique intracellular structures, called endosomes, in animal models of sporadic and familial forms of the disease. Earlier studies proved that in both models the actual stress condition could result in increased calcium in mitochondria and endoplasmic reticulum of vulnerable motoneurons, suggesting that elevated intracellular calcium may be the common pathway leading to the clinically iden-

tical manifestations of sporadic and familial ALS. In this study we documented that endosomes had the capacity to sequester large loads of calcium, concentrate the majority of intracellular calcium at the terminals, and could establish connection to the extracellular space. These findings imply that endosomes might effectively contribute to the compartmentalization of intracellular calcium and relieve other intracellular structures from stress due to the excess calcium load. At present it is not clear why such endosomes do form selectively in resistant nerve terminals. However, motoneuronal vulnerability correlates with the lack of calcium binding proteins, calbindin D_{28K} and/or parvalbumin, and motoneurone correlates with the presence of the calcium binding proteins and the development of endosomes in models of familial and sporadic ALS.

References

1. Orrenius S and Nicotera P. *J Neural Trans* **43(Suppl.)**, 1–11 (1994).
2. Siklos L, Engelhardt J, Harati Y *et al. Ann Neurol* **39**, 203–216 (1996).
3. Engelhardt JI, Siklos L, Komuves L *et al. Synapse* **20**, 185–199 (1995).
4. Gurney ME, Pu H, Chiu AY *et al. Science* **264**, 1772–1775 (1994).
5. Siklos L, Engelhardt JI, Alexianu ME *et al. J Neuropathol Exp Neurol* **57**, 571–587 (1998).
6. Grohovaz F, Bossi M, Pezzati R *et al. Proc Natl Acad Sci USA* **93**, 4799–4803 (1996).
7. Siklos L, Kuhnt U, Parducz A and Szerdahelyi P. *Neuroscience* **79**, 1013–1022 (1997).
8. Gunter TE, Gunter KK, Sheu S-S and Gavin CE. *Am J Physiol* **267**, C313–C339 (1994).
9. Golovina VA and Blaustein MP. *Science* **275**, 1643–1648 (1997).
10. Volpe P, Krause K-H, Hashimoto S *et al. Proc Natl Acad Sci USA* **85**, 1091–1095 (1988).
11. Anderson RGW. *Proc Natl Acad Sci USA* **90**, 10909–10913 (1993).
12. Meldolesi J, Krause K-H and Michalak M. *Cell Calcium* **20**, 83–86 (1996).
13. Takei K, Mundigl O, Daniell L and De Camilli P. *J Cell Biol* **133**, 1237–1250 (1996).
14. Gad H, Löw P, Zotova H *et al. Neuron* **21**, 607–616 (1998).
15. von Gersdorff H and Matthews G. *Nature* **370**, 652–655 (1994).
16. Brodin L, Löw P, Gad H *et al. Eur J Neurosci* **9**, 2503–2500 (1997).
17. Bruijn LI, Housewart MK, Kato S *et al. Science* **281**, 1851–1854 (1998).
18. Roy J, Minotti S, Dong L *et al. J Neurosci* **18**, 9673–9684 (1998).
19. Robberecht W, Sapp P, Viaene MK *et al. J Neurochem* **62**, 384–387 (1994).
20. Rothstein JD. *Neurology* **47(Suppl.)**, S19–S26 (1996).
21. Smith RG, Siklos L, Alexianu ME *et al. Neurology* **47(Suppl.)**, S40–S46 (1996).
22. Mosier DR, Baldelli P, Delbono O *et al. Ann Neurol* **37**, 102–109 (1995).
23. Alexianu ME, Ho B-K, Mohamed AH *et al. Ann Neurol* **36**, 846–858 (1994).

ACKNOWLEDGEMENTS: We thank Mark E. Gurney and Teepu Siddique in the Northwestern Medical School, Chicago, IL, for their support in this study. This work was funded by grants from Muscular Dystrophy Association, FIRCA, Cephalon Inc., US-Hungary Science and Technology Program, OTKA (026239), AKP and ETT (053/T-04).

Received 26 May 1999; accepted 12 June 1999

II.

Acta Neuropathol (2000) 99:517–524

REGULAR PAPER

László Siklós · József I. Engelhardt
Andrew G. Reaume · Richard W. Scott
Róbert Adalbert · Izabella Obál · Stanley H. Appel

Altered calcium homeostasis in spinal motoneurons but not in oculomotor neurons of SOD-1 knockout mice

Received: 31 May 1999 / Revised, accepted: 16 August 1999

Abstract SOD-1-deficient mice demonstrate no loss of motoneurons but are still vulnerable to axotomy and ischemic insults. To investigate possible reasons for vulnerability of motoneuron populations, we studied changes in ultrastructural calcium distribution during maturation in spinal- and oculomotor neurons in SOD-1$^{-/-}$ mice. Between 3 and 11 months the cytoplasmic component of the intracellular calcium changed at a lower rate in spinal motoneurons and motor axon terminals in the interosseus muscle of SOD-1$^{-/-}$ animals compared to wild-type controls. No such dissimilarities were noted in the oculomotor system, or in mitochondrial calcium contents of either cell type. These data suggest that the lack of SOD-1 may be associated with vulnerability to insult by depletion of non-mitochondrial calcium stores selectively in motoneurons lacking parvalbumin and/or calbindin D28K.

Key words Calcium · SOD-1 · Knockout mouse · Motoneuron · Parvalbumin

L. Siklós · J. I. Engelhardt · S. H. Appel (✉)
Department of Neurology, Baylor College of Medicine,
One Baylor Plaza, Houston, TX 77030, USA
e-mail: sappel@bcm.tmc.edu,
Tel.: +1-713-7984072, Fax: +1-713-7983854

L. Siklós · R. Adalbert
Institute of Biophysics, Biological Research Center,
Szeged, Hungary

J. I. Engelhardt · I. Obál
Department of Neurology,
Albert Szent-Györgyi School of Medicine, Szeged, Hungary

A. G. Reaume · R. W. Scott
Department of Molecular Biology, Cephalon, Incorporated,
West Chester, Pennsylvania, USA

L. Siklós · J. I. Engelhardt · R. Adalbert · I. Obál
Joint Research Program of the Biological Research Center
of the Hungarian Academy of Sciences
and Albert Szent-Györgyi School of Medicine, Szeged, Hungary

Introduction

Impaired calcium homeostasis of spinal motoneurons has been documented in amyotrophic lateral sclerosis (ALS), a relentlessly progressive, lethal neurological disease [12, 34]. One form of familial ALS has been attributed to missense mutations in the gene encoding Cu/Zn superoxide dismutase (SOD-1) [32] and transgenic models of these mutations have been developed [14, 41]. Ventral horn sections from two strains with different SOD-1 mutations ($G^{93}\rightarrow A$, $G^{85}\rightarrow R$) contained inclusions, strongly stained with SOD-1 antibody, regardless of the level of normal SOD-1 activity [4]. Although these results suggest that generalized oxidative stress may not be the main factor mediating toxicity, neuronal vulnerability still appears to depend on calcium entry and deficiency of cytosolic calcium binding proteins [30]. Accordingly, increased calcium accumulation was detected in spinal motoneurons of SOD-1 transgenic animals bearing $G^{93}\rightarrow A$ mutation [33], suggesting that elevated calcium may be a common pathway leading to the clinically identical manifestations of sporadic and familial ALS.

To determine how animals respond to a loss of SOD-1 activity, mice deficient in SOD-1 enzyme were developed [28] and introduced into different experimental paradigms [4,22]. Although SOD-1$^{-/-}$ animals were more susceptible to axonal injury [28] or to stroke [22] compared to wild type normals, unexpectedly, they developed normally, and exhibited no detectable signs of oxidative damage [28]. To determine whether the normal motor development and increased vulnerability of SOD$^{-/-}$ animals could be associated with specific alterations of calcium homeostasis, we analyzed the distribution of intracellular calcium ($[Ca^{2+}]_i$) in motoneuron populations showing different susceptibility to mutant SOD-1 defect [33]. Calcium distribution of spinal and oculomotor neurons as well as motor axon terminals innervating interosseus (IOS) and external eye muscles were studied by electron microscopy at the ages of 3 and 11 months. No changes in cytoplasmic calcium were noted between 3 and 11 months in oculo-

motor neurons. However, between 3 and 11 months, calcium in the cytoplasm and endoplasmic reticulum of spinal motoneurons and motor axon terminals in the IOS muscle failed to follow the age-associated increase noted in wild-type controls.

Materials and methods

Animals

SOD-1 knockout animals were developed as described earlier [28]. Using homologous recombination in embryonic stem cells the entire coding sequence of the mouse SOD-1 gene has been deleted. These mutant cells were used to create mice homozygous for the SOD-1 deletion (SOD-1$^{-/-}$). Blood samples were used to confirm that the targeted deletion of SOD-1 gene resulted in no detectable amount of Cu/Zn SOD protein and only a minor level of enzyme activity [28].

Specimen preparation for electron microscopic calcium histochemistry

SOD-1$^{-/-}$ and wild-type control mice were selected at 3 and 11 months months of age (four animals in each group) to characterize the subcellular calcium distribution in spinal- and oculomotor neurons, together with motor nerve terminals innervating IOS and external eye muscles. Animals were transcardially perfused under Metofane anesthesia first with 90 mM potassium oxalate (pH 7.4 with KOH) followed by 3% glutaraldehyde containing 90 mM potassium oxalate, adjusted to pH 7.4 with KOH [2, 3]. The following samples were dissected out: (a) randomly selected samples from the hindlimb interosseus muscle, (b) one of the external eye muscles, regularly the superior rectus muscle from the right eye, as a whole piece, (c) an approximately 0.5-mm-thick transverse section from the lumbar segment of the spinal cord, and (d) a laterally sectioned tissue slice, with characteristic dimension of 1 mm, from the brain stem of the right hemisphere containing the oculomotor nucleus. Samples were evaluated immediately following dissection under a stereomicroscope for optimal fixation, and all the specimens showing any sign of suboptimal tissue preservation by the perfusion fixation were *a priori* excluded from further analysis. All samples were placed in the same oxalate-containing fixative for an additional 24 h at 4 °C. Tissue blocks were then rinsed for 15 min in 7.5% sucrose containing 90 mM potassium oxalate followed by fixation in 2% potassium pyroantimonate, 1% osmic acid and 0.01 N acetic acid for 2 h (4 °C). Following postfixation, tissue blocks were rinsed in distilled water, dehydrated in graded series of ethanol, processed through propylene oxide, infiltrated in Durcupan ACM, and finally, cured at 56 °C for 2 days.

Semithin sections were first cut on an RMC-MT-7 ultramicrotome and screened in a light microscope for the presence of nerve terminals or large motoneurons in muscle samples or brain tissue, respectively, to determine the "onset" point of sampling. To ensure a lack of bias in determining observation fields for ultrastructural analysis, a randomly selected number of 0.5-μm-thick sections were cut ($1 < n < 20$) and discarded, then from this new starting point ultrathin sections were systematically obtained at 20-μm intervals [8, 13] for analysis in a Philips CM12, or Zeiss CEM 902 transmission electron microscope.

The applied oxalate-pyroantimonate procedure to trap and visualize the subcellular distribution of calcium resulted in electron-dense precipitates, easily recognizable by conventional transmission electron microscopy. The method is widely used for ultrastructural calcium distribution studies [39].

Determination of the volume fraction of calcium-containing precipitates

All the sections prepared from muscle samples were screened exhaustively under a microscope using low magnification (×5000–×7000). If endplates were encountered, they were photographed without any selection at a magnification between ×10,000 and ×20,000, and the negatives were further enlarged by ×2.7. This data collection procedure was continued until 15–20 endplates were photographed from a particular muscle/animal.

All sections prepared from different brain regions were screened in the survey image mode of the microscope (×300–×1100). If a motoneuron was found, three non-overlapping cytoplasmic views were photographed without any selection at a magnification between ×10,000 and ×20,000, and the negatives were further enlarged by ×2.7. From each spinal cord and oculomotor nucleus three to five motoneurons were photographed for analysis.

From ultrathin sections of muscle and brain samples the volume fraction of calcium-containing precipitates were determined according to standard stereological procedures [23]. Since calcium-containing deposits differ in shape and size, simple grain counts were an imprecise measure of the amount of granules in the tissue. Instead, we determined the actual volume of the irregularly shaped deposits in relation to a selected reference (container) space such as mitochondrial volume or axoplasmic volume. These volume-to-volume ratios could be determined on electron microscopic prints with a simple point counting procedure [23]. To determine mitochondrial calcium volume fractions, mitochondrial profiles were marked in the axoplasm of motor nerve terminal or in the cytoplasm of motoneuron perikarya and points of the sampling grid (superimposed randomly on the photomicrographs) lying over calcium-containing electron-dense precipitates (P_{Ca}) as well as lying over mitochondrial profiles (P_{mit}) were counted, then pooled to each animal/muscle type (ΣP_{Ca}, ΣP_{mit}). The $\Sigma P_{Ca}/\Sigma P_{mit}$ ratio was used to characterize the mitochondrial calcium volume fraction of that particular muscle/animal. Similar calculations were used to characterize non-mitochondrial calcium volume fraction in motor axon terminals and perikarya of motoneurons, but in this case sample grid points lying over cytoplasmic, or axoplasmic area, but not over mitochondria, were used to sample the reference space ($\Sigma P_{non\text{-}mit}$). The $\Sigma P_{Ca}/\Sigma P_{non\text{-}mit}$ ratio was used to characterize the non-mitochondrial calcium volume fraction in motor nerve terminals and cell bodies.

Results

Non-mitochondrial calcium volume fractions in perikarya of spinal motoneurons and motor axon terminals in the IOS muscle

The non-mitochondrial calcium volume fractions were determined using a reference space by delineating the appropriate profiles of perikarya or axon terminals on electron microscopic prints, and by excluding all mitochondrial compartments. Thus, these data contained contributions from the cytoplasm, endoplasmic reticulum, Golgi apparatus, and synaptic vesicles. The calcium volume fraction numbers were usually smaller in the motor axon terminals than in the cell bodies. We found a steep increase with age for wild-type animals both in the perikarya and motor nerve terminals (Fig. 1 A, C). With these data as a physiological baseline (accounting for the effect of aging), the corresponding age-matched values from the SOD-1 knockout animals were always considerably smaller. This difference increased with age, and by the age of 11 months reached a highly significant level (Fig. 1 A, C). Thus, these neuronal structures in mice lacking the SOD-

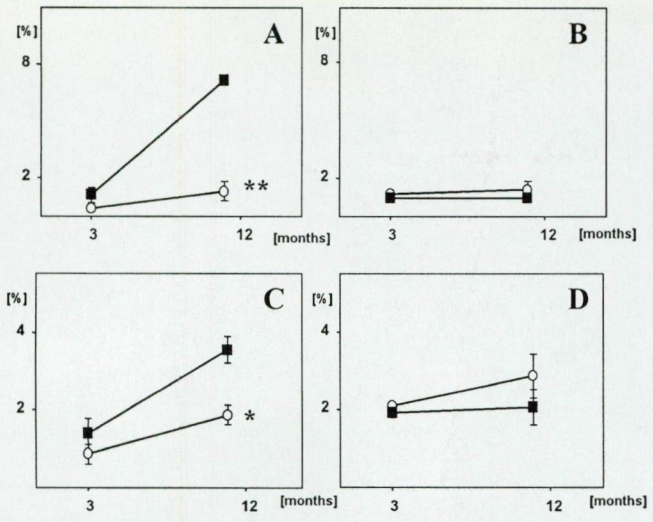

Fig. 1 Non-mitochondrial calcium volume fractions were determined (as % of the volume of calcium precipitates in relation to the cytoplasmic volume) in perikarya of spinal motoneurons (**A**), in motoneurons of oculomotor nucleus (**B**), as well as in motor nerve terminals innervating interosseus muscle (**C**) and external eye muscles (**D**) at ages 3 and 11 months of SOD knockout mice (*open circles*) and wild type control animals (*solid rectangles*). Cytoplasmic calcium contents of SOD$^{-/-}$ mice were lower than controls in spinal motoneurons and in motor nerve terminals of the interosseus muscle at both time points, and this difference reached a statistically significant level at age 11 months of animals ($*P < 0.05$, $**P < 0.01$). No significant differences between the cytoplasmic calcium volume fraction values of the oculomotor neurons of SOD$^{-/-}$ and wild-type mice could be demonstrated at any time point observed

1 gene became gradually depleted of calcium compared to physiological controls (Fig. 2 A–D).

Non-mitochondrial calcium volume fractions in perikarya and axon terminals of oculomotor neurons

In oculomotor neurons, we saw neither an age-dependent change nor large differences between the calcium volume fraction values in perikarya and motor axon terminals of wild-type animals (Fig. 1 B, D). Furthermore, the corresponding data from SOD-1 knockout and wild-type mice did not exhibit statistical differences at either time point investigated. Electron micrographs from SOD-1$^{-/-}$ and wild-type animals, both at early and late time points, clearly displayed similar tissue appearance and $[Ca^{2+}]_i$ distribution (Fig. 3 A–D).

Calcium volume fractions in mitochondria of spinal and oculomotor neurons

In perikarya and motor axon terminals, mitochondrial calcium volume fractions were assayed by point counting methods on electron micrographs using mitochondrial volume as reference space and expressing the volume of electron-dense deposits (representing calcium content of the tissue) as percentage of the reference volume. These volume fraction data showed a general tendency to increase with age (Table 1). Since the aim of the present study was not to analyze the effect of the aging process on the mitochondrial calcium content, all the data characterizing SOD-1$^{-/-}$ animals were simply compared to the corresponding age-matched controls. At each age and in each tissue compartment group, the mitochondrial calcium volume fraction data of SOD-1 knockout animals were not significantly different (with two-tailed Student's *t*-test) from those of wild-type mice, i.e., these values were independent of the presence of the SOD-1 gene in the animals.

Discussion

Specificity of the histochemical reaction

To determine subcellular distribution of calcium in motor nerve terminals and perikarya of motoneurons, deeply anesthetized animals were transcardially perfused with oxalate anion-containing fixative, to trap tissue calcium and preserve the structural details. The procedure resulted in fine electron dense precipitates over the cytoplasm and membrane enclosed organelles (Figs. 2, 3). This fixation protocol is well documented [9, 10, 17, 20, 24, 37], provides good ultrastructural preservation of the entire volume of the sample, and does not introduce structural alterations compared to conventional perfusion fixation [35]. The specificity of the chemical reaction was regularly controlled by electron spectroscopic imaging [1] (data not shown).

Effect of aging on neuronal calcium of wild-type animals

Intrinsic cellular properties appear to differentially affect neuronal $[Ca^{2+}]_i$ levels during aging [19, 38]. In the present study we have shown that cytoplasmic calcium concentrations increase with age in wild-type spinal motoneurons, while no changes are noted in oculomotor neurons of the same animals (Fig. 1). In our earlier studies we demonstrated, that mouse spinal motoneurons do not stain with monoclonal antibody against parvalbumin, while oculomotor neurons do stain to a faint-to-moderate extent [5, 33]. Thus, our present observation suggests that stabilization of calcium homeostasis during aging is associated with the presence of certain cytoplasmic calcium binding proteins. This is in accordance with the proposal [7] that the composition and concentration of cytosolic calcium buffers, exemplified by calcium binding proteins, afford neuroprotection.

Selective impairment of cytoplasmic calcium buffering in spinal motoneurons of SOD-1$^{-/-}$ mice

Mitochondria in motoneurons appear to be spared in SOD-1$^{-/-}$ animals, since no change in their calcium content

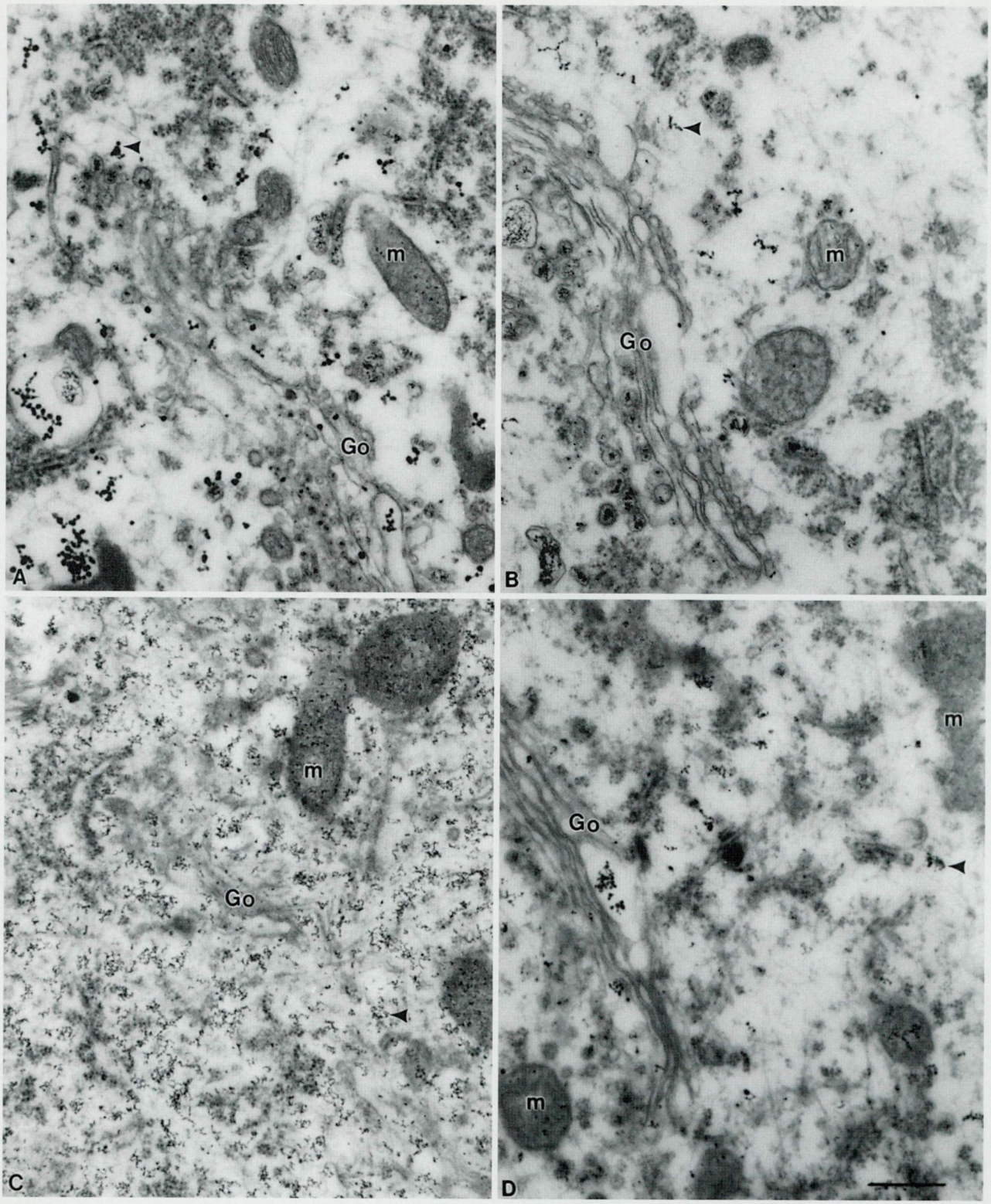

Fig. 2 Electron micrograph of spinal motoneurons from wild-type (**A**, **C**) and SOD-1$^{-/-}$ (**B**, **D**) mice after oxalate-pyroantimonate fixation. At 3 months of age the difference between the calcium distribution in motoneurons of wild-type (**A**) and SOD-1$^{-/-}$ mice (**B**), represented by the electron-dense precipitates, is not obvious. At age of 11 months an increased number of precipitates can be seen in wild-type motoneurons (**C**), while in SOD-1$^{-/-}$ animals no such increase is present (**D**) (*m* mitochondrion, *Go* Golgi apparatus, *arrowhead* calcium deposits). *Bar* 1 μm

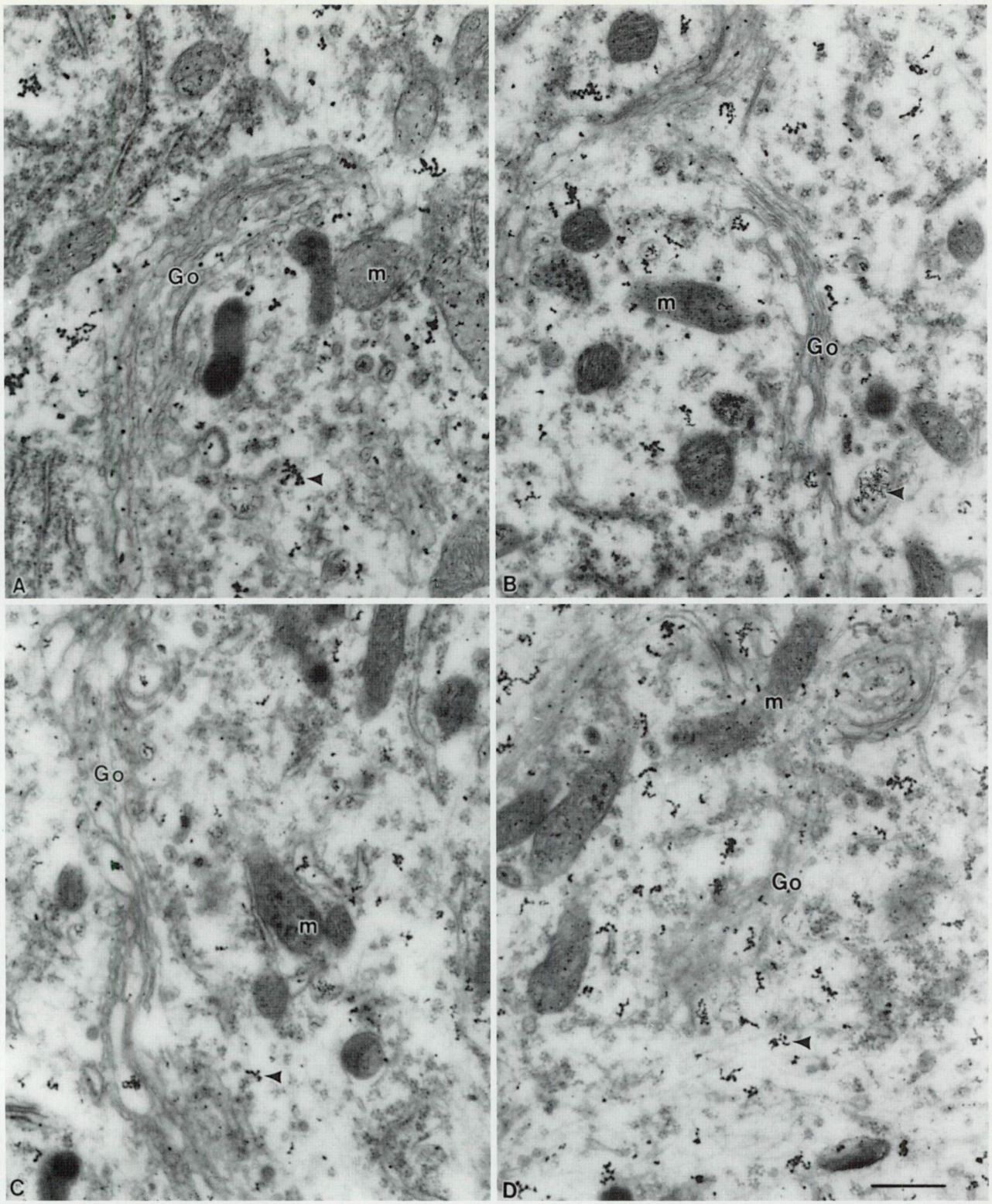

Fig. 3 Electron micrographs of oculomotor neurons from wild-type (**A**, **C**) and SOD-1$^{-/-}$ (**B**, **D**) mice after oxalate-pyroantimonate fixation. No difference can be seen between the calcium distribution of motoneurons from control- and SOD-1$^{-/-}$ mice at either 3 months (**A**, **B**) or 11 months (**C**, **D**) of age (*m* mitochondrion, *Go* Golgi apparatus, *arrowhead* calcium deposits). *Bar* 1 μm

Table 1 Calcium volume fractions in mitochondria of motoneurons as a function of age of SOD knockout ($^{-/-}$) and wild-type control animals. Mitochondrial calcium volume fraction ($\times 10^{-3}$) in perikarya of spinal motoneurons (lumbar segment) and motoneurons of oculomotor nucleus, as well as in motor nerve terminals in the interosseus muscle and external eye muscles were determined at 3 months and 11 months age of animals. In each group (with one exception, as shown), data were obtained from two to four animals and expressed as mean ± SEM. None of the differences between the corresponding age-matched wild type and $^{-/-}$ groups are statistically significant

Tissue	SOD$^{-/-}$		Wild type	
	3 months	11 months	3 months	11 months
Spinal cord	36.55 ± 4.37	77.34 ± 31.75	30.15 ± 9.56	98.79 ± 47.09
Interosseus muscle	18.80 ± 9.81	52.75 ± 20.82	18.94 ± 6.57	64.40 ± 6.76
Oculomotor nucleus	38.42 ± 17.00	31.90 ± 8.29	23.72 ± 6.57	60.04 ($n = 1$)
External eye muscles	13.63 ± 1.05	66.39 ± 3.91	12.22 ± 5.60	23.15 ± 12.18

(Table 1) or ultrastructure was noted. Given that the main source of $O^{\bullet -}$ is the mitochondrial respiratory cycle [29], and SOD-2 (Mn-SOD) is present as the main defense system in mitochondria [26], it is likely that very little $O^{\bullet -}$ leaks to the cytosol under physiological (unchallenged) conditions. Neither assay of common end-products of oxidative damage (brain tissue levels of lipid peroxidation and protein carbonyl content) revealed any change in the SOD-1$^{-/-}$ mice compared to wild-type controls [28].

Earlier studies on SOD-1 transgenic animals demonstrated a large increase in $[Ca^{2+}]_i$ in spinal motoneurons as a consequence of abnormal SOD-1 enzymatic operation [33]. Thus, the observed reduction of $[Ca^{2+}]_i$ in the same neuronal population of SOD-1-deficient animals was rather unexpected. The lack of SOD-1 activity in the cytosol and the resultant primary breakdown route of $O^{\bullet -}$ radicals through the reaction $O^{\bullet -} + NO^{\bullet} \rightarrow ONOO^-$ [40], would imply that (i) the $O^{\bullet -}$ level in the cytosol is slightly increased, (ii) the cytosolic $ONOO^-$ concentration is proportionally increased, and (iii) the cytosolic $NO^{\bullet}$ concentration is decreased (since the competition for $O^{\bullet -}$ would be now dominated by $NO^{\bullet}$ alone). Thus, it is reasonable to assume that concentration changes of these compounds may influence cytoplasmic calcium levels, and previous studies support this postulate, as detailed in the following.

Effects of $O^{\bullet -}$ on $[Ca^{2+}]_i$ homeostasis were directly studied on isolated sarcoplasmic reticulum (SR) preparations, and $O^{\bullet -}$ produced less calcium accumulation in SR due to increased calcium permeability, and not due to an inhibited calcium pump (Ca-ATPase) [27]. In calf pulmonary artery endothelial cells, $ONOO^-$ donors selectively decreased agonist-stimulated influx of external Ca^{2+}, and depleted internal stores of releasable Ca^{2+} [11]. In our studies we did not expect a major increase of $ONOO^-$, since there was minimal damage to mitochondria, and minimal leakage of $O^{\bullet -}$ was expected. Further, the absence of SOD-1 should have minimized protein nitration associated with $ONOO^-$ [16]. Finally, $NO^{\bullet}$ has been documented to modulate Ca^{2+} mobilization from internal stores in human platelets [31], and function as a sensor for $[Ca^{2+}]_i$ [36]. Thus, if decreasing concentrations of $NO^{\bullet}$ have any effect, they should facilitate the release from the calcium stores and deplete such stores. The above processes, acting either individually, or together, could reduce the intracellular storage capacity of membrane enclosed organelles. Consequently, a new total $[Ca^{2+}]_i$ level set point would have been achieved. This new set point would be determined solely by the storage capacity of the cytosolic components (concentration of relevant calcium binding proteins), and might explain the low calcium levels in spinal motoneurons of SOD-1$^{-/-}$ animals. Another unexpected feature of animals lacking SOD-1, the main cytoplasmic defense system against oxidative stress, is that these mice develop normally, although they are prone to injury. This can be understood if we assume that the lowered $[Ca^{2+}]_i$ set point of SOD-1$^{-/-}$ spinal motoneurons, compared to age-matched controls, which still can be in the physiological range, may not be optimal for certain cellular functions, such as synapse remodeling [18]. Indeed, in earlier experiments, lowering of $[Ca^{2+}]_i$ using voltage gated calcium channel blockers was shown to suppress neurite elongation, as well as retraction of growth cone lamellipodia and filopodia in identified molluscan neurons [25], or could impair neuromuscular synapse formation in a retinal embryonic neuron-myotube co-culture system [36]. Furthermore, experimental depletion of $[Ca^{2+}]_i$ stores of dorsal root ganglion neurons with thapsigargin could similarly prevent neurite outgrowth [21]. These results imply that a suitable level of $[Ca^{2+}]_i$ and intact calcium stores are equally necessary for neurite elongation and formation of new synapses. Recent electrophysiological and histopathological characterization of mature SOD-1$^{-/-}$ mice revealed a slow development of mild, chronic peripheral hindlimb axonopathy (Flood, personal communication), a moderate decline in motor unit numbers, but only a negligible change in the motor unit size (Shefner, personal communication). This impaired sprouting noted in the main hindlimb muscles of SOD-1$^{-/-}$ animals can be readily explained by the observed reduction of $[Ca^{2+}]_i$ in spinal motoneurons and by the possible compromised function of their $[Ca^{2+}]_i$ stores.

Cytosolic calcium buffering can protect from calcium depletion in oculomotor neurons of SOD-1$^{-/-}$ mice

Oculomotor and spinal motoneurons differ with respect to the presence of parvalbumin, which is only present as a

possible cytosolic calcium buffer in oculomotor neurons. Thus, in oculomotor neurons, assuming the same effect of the $O^{\bullet-}$ breakdown components, calcium ions released from the "leaky" internal stores can be immediately captured by the calcium binding protein molecules in the vicinity of the release sites and recycled into the stores, escaping the extrusion pumps, as proposed by Hofer et al. [15]. Furthermore, even with compromised vesicular buffers, due to the relative high proportion of the cytosolic buffer capacity, the new $[Ca^{2+}]_i$ level set point of these neurons can not be changed as strongly as in the case of cells lacking this capacity.

The increased susceptibility of SOD-$1^{-/-}$ animals to neuronal injury can possibly be explained on the basis that their $[Ca^{2+}]_i$ buffer capacity is compromised, and that a major component of the cytosolic free radical defense mechanism is missing. Thus, any injury leading to excess calcium influx and free radical production can overwhelm the cooperative free radical and calcium homeostasis systems, which might have a less devastating effect in those cells, where the deviation from the optimal physiological condition is less prominent, i.e., in neurons abundant in relevant calcium binding proteins.

Acknowledgements This work was supported by grants from the Muscular Dystrophy Association, Cephalon, Inc., the Fogarty International Research Collaboration Award (FIRCA), the US-Hungarian Science and Technology Joint Fund (MAKA), the Hungarian Academy of Sciences (AKP), the Hungarian Ministry of Welfare (ETT) and the National Scientific Research Fund of Hungary (OTKA).

References

1. Bauer R (1988) Electron spectroscopic imaging: an advanced technique for imaging and analysis in transmission electron microscopy. Methods Microbiol 20: 113–146
2. Borgers M, De Brabander DM, Van Reempts DJ, Awouters F, Jacob WA (1977) Intranuclear microtubules in lung mast cells of guinea pigs in anaphylactic shock. Lab Invest 39: 1–8
3. Borgers M, Thoné EF, Van Neuten JM (1981) The subcellular distribution of calcium and the effects of calcium-antagonists as evaluated with a combined oxalate-pyroantimonate technique. Acta Histochem S24: 327–332
4. Bruijn LI, Houseweart MK, Kato S, et al (1998) Aggregation and motor neuron toxicity of an ALS-linked SOD1 mutant independent from wild-type SOD1. Science 281: 1851–1854
5. Celio MR (1990) Calbindin D28K and parvalbumin in the rat nervous system. Neuroscience 35: 375–475
6. Clementi E (1998) Role of nitric oxide and its intracellular signalling pathways in the control of Ca^{2+} homeostasis. Biochem Pharmacol 55: 713–718
7. Clementi E, Racchetti G, Melino G, Meldolesi J (1996) Cytosolic Ca^{2+} buffering, a cell property that in some neurons markedly decreases during aging, has a protective effect against NMDA/nitric oxide-induced excitotoxicity. Life Sci 59: 389–397
8. Cruz-Orive LM (1988) On the precision of systematic sampling. J Microsc 30: 1–34
9. Dux E, Mies H, Hossmann K-A, Siklós L (1987) Calcium in the mitochondria followung brief ischemia of gerbil brain. Neurosci Lett 78: 295–300
10. Dux E, Oschlies U, Uto A, et al (1996) Serum prevents glutamate-induced mitochondrial calcium accumulation in primary neuronal cultures. Acta Neuropathol 92: 264–272
11. Elliott SJ (1996) Peroxynitrite modulates receptor-activated Ca^{2+} signaling in vascular endothelial cells. Am J Physiol 270: L954–L961
12. Engelhardt JI, Siklós L, Kömüves L, Smith RG, Appel SH (1995) Passive transfer of amyotrophic lateral sclerosis (ALS) immunoglobulin to mice selectively increases intracellular calcium and induces ultrastructural changes in motonuerons. Synapse 20: 185–199
13. Gundersen HJG, Jensen EB (1987) The efficiency of systematic sampling in stereology and its prediction. J Microsc 147: 229–263
14. Gurney ME, Pu H, Chiu AY, et al (1994) Motor neuron degeneration in mice that express a human Cu,Zn superoxide dismutase mutation. Science 264: 1772–1775
15. Hofer AM, Landolfi B, Debellis L, Pozzan T, Curci S (1998) Free $[Ca^{2+}]$ dynamics measured in agonist-sensitive stores of single living intact cells: a new look at the refilling process. EMBO J 17: 1986–1995
16. Ischiropoulos H, Zhu L, Chen J, et al (1992) Peroxynitrite-mediated tyrosine nitration catalyzed by superoxide dismutase. Arch Biochem Biophys 298: 431–437
17. Kamphuis W, Huisman E, Wadman WJ, Bergkamp FJ, Lopes da Silva FH (1989) Transient increase of cytoplasmic calcium concentration in the rat hippocampus after kindling-induced seizures. An ultrastructural study with the oxalate-pyroantimonate technique. Neuroscience 29: 667–674
18. Kater SB, Mills LR (1991) Regulation of growth cone behavior by calcium. J Neurosci 11: 891–899
19. Kirischuk S, Verkhratsky A (1996) Calcium homeostasis in aged neurones. Life Sci 59: 451–459
20. Kittel A, Siklós L, Thuróczy G, Somosy Z (1996) Qualitative enzyme histochemistry and microanalysis reveals changes in ultrastructural distribution of calcium and calcium activated ATPases after microwave irradiation of the medial habenula. Acta Neuropathol 92: 362–368
21. Kocsis JD, Rand MN, Lankford KL, Waxman SG (1993) Intracellular calcium mobilization and neurite outgrowth in mammalian neurons. J Neurobiol 25: 252–264
22. Kondo T, Reaume AG, Huang T-T, et al (1997) Reduction of CuZn-superoxide dismutase activity exacerbates neuronal injury and edema formation after transient focal cerebral ischemia. Neuroscience 17: 4180–4189
23. Mayhew TM (1992) A review of recent advances in stereology for quantifying neuronal structure. J Neurocytol 21: 313–328
24. Mata M, Staple J, Fink DJ (1986) Changes in intra-axonal calcium distribution following nerve crush. J Neurobiol 17: 449–467
25. Mattson MP, Kater SB (1987) Calcium regulation of neurite elongation and growth cone mobility. J Neurosci 7: 4034–4043
26. Michiels C, Raes M, Toussaint O, Remacle J (1994) Importance of Se-glutathione peroxidase, catalase, and Cu/Zn-SOD for cell survival against oxidative stre˜˜s. Free Radic Biol Med 17: 235–248
27. Okabe E, Odajima C, Taga R, Kukreja RC, Hess ML, Ito H (1988) The effect of oxygen free radicals in calcium permeability and calcium, loading at steady state in cardiac sacoplasmic reticulum. Mol Pharmacol 34: 388–394
28. Reaume AG, Elliott JL, Hoffmann EK, et al (1996) Motor neurons in Cu/Zn superoxide dismutase-deficient mice develop normally but exhibit enhanced cell death after axonal injury. Nat Genet 13: 43–47
29. Richter C, Gogvadze V, Laffranchi R, et al (1995) Oxidants in mitochondria: from physiology to diseases. Biochim Biophys Acta 1271: 67–74
30. Roy J, Minotti S, Dong L, Figlewicz DA, Durham HD (1998) Glutamate potentiates the toxicity of mutant Cu/Zn-superoxide dismutase in motor neurons by postsynaptic calcium-dependent mechanisms. J Neurosci 18: 9673–9684
31. Sang K-HLQ, Lantoine F, Devynck M-A (1996) Influence of authentic nitric oxide on basal cytosolic $[Ca^{2+}]$ and Ca^{2+} release from internal stores in human platelets. Br J Pharmacol 119: 1361–1366

32. Siddique T, Isozumi K (1996) From the discovery of genetic linkage to chromosome 21 and mutations in SOD1 to the molecular basis of familial amyotrophic lateral sclerosis. In: Nakano I, Hirano A (eds) Amyotrophic lateral sclerosis: progress and perspectives in basic research and clinical applications. Elsevier, Amsterdam, pp 266–275
33. Siklós L, Engelhardt JI, Alexianu ME, Gurney ME, Siddique T, Appel SH (1998) Intracellular calcium parallels motoneuron degeneration in SOD-1 mutant mice. J Neuropathol Exp Neurol 57: 571–587
34. Siklós L, Engelhardt JI, Harati Y, Smith RG, Joo F, Appel SH (1996) Ultrastructural evidence for altered calcium in motor nerve terminals in amyotrophic lateral sclerosis. Ann Neurol 39: 203–216
35. Siklós L, Kuhnt U, Párducz A, Szerdahelyi P (1997) Intracellular calcium redistribution accompanies changes in total tissue Na, K and water during the first two hours of in vitro incubation of hippocampal slices. Neuroscience 79: 1013–1022
36. Suarez-Isla BA, Pelto DJ, Thompson JM, Rapoport SI (1984) Blockers of calcium permeability inhibit neurite extension and formation of neuromuscular synapses in cell culture. Dev Brain Res 14: 263–270
37. Suzuki S, Sugi H (1980) Evidence for extracellular localization of activator calcium in dog coronary artery smooth muscle as studied by the pyroantimonate method. Cell Tissue Res 257: 237–246
38. Verkhratsky A. Toescu EC (1998) Calcium and neuronal ageing. Trend Neurosci 21: 2–7
39. Vöhringer P, Nindl G, Aich B, Körtje K-H, Rahmann H (1995) Comparative methodological investigations on the cytochemical localization of calcium in brain and inner ear of cichlid fish. Microsc Res Tech 31: 317–325
40. Warner RR (1994) Superoxide dismutase, aging, and degenerative disease. Free Radic Biol Med 17: 249–258
41. Wong PC, Pardo CA, Borchelt DR, et al (1995) An adverse property of a familial ALS-linked SOD1 mutation causes motor neuron disease characterized by vacuolar degeneration of mitochondria. Neuron 14: 1105–1116

III.

Acta Neuropathologica

DOI 10.1007/s00401-001-0485-5

Regular Paper

DL-Homocysteic acid application disrupts calcium homeostasis and induces degeneration of spinal motor neurons in vivo

Róbert Adalbert[1], József I. Engelhardt[2] and László Siklós[1,✉]

(1) Institute of Biophysics, Biological Research Center, P.O. Box 521, 6701 Szeged, Hungary

(2) Department of Neurology, University of Szeged, Szeged, Hungary

✉ E-mail: siklos@nucleus.szbk.u-szeged.hu
Phone: +36-62-432080170
Fax: +36-62-433133

Received: 9 May 2001 / **Revised:** 27 July 2001 / **Accepted:** 3 October 2001 / **Published online:** 23 February 2002

Abstract. Excitotoxicity, autoimmunity and free radicals have been postulated to play a role in the pathomechanism of amyotrophic lateral sclerosis (ALS), the most frequent motor neuron disease. Altered calcium homeostasis has already been demonstrated in Cu/Zn superoxide dismutase transgenic animals, suggesting a role for free radicals in the pathogenesis of ALS, and in passive transfer experiments, modeling autoimmunity. These findings also suggested that yet-confined pathogenic insults, associated with ALS, could trigger the disruption of calcium homeostasis of motor neurons. To test the possibility that excitotoxic processes may also be able to increase calcium in motor neurons, we applied the glutamate analogue DL-homocysteic acid to the spinal cord of rats in vivo and analyzed the calcium distribution of the motor neurons over a 24-h survival period by electron microscopy. Initially, an elevated cytoplasmic calcium level, with no morphological sign of degeneration, was noticed. Later, increasing calcium accumulation was seen in different cellular compartments with characteristic features of alteration at different survival times. This calcium accumulation in organelles was paralleled by their progressive degeneration, which culminated in cell death by the end of the observation time. These findings confirm that increased calcium also plays a role in excitotoxic lesion of motor neurons, in line with previous studies documenting the involvement of calcium ions in motor neuronal injury in other models of the disease as well as elevated calcium in biopsy samples from ALS patients. We suggest that intracellular calcium might be responsible for the interplay between the different pathogenic processes resulting in a uniform clinicopathological picture of the disease.

Keywords. Calcium - Excitotoxicity - Motor neuron - DL-Homocysteic acid

Introduction

Amyotrophic lateral sclerosis (ALS) is a neurodegenerative disorder characterized by progressive loss of upper and lower motor neurons, leading to paralysis, respiratory failure and death [14]. ALS occurs in both sporadic (sALS) and familial (fALS) forms, which are clinically and pathologically similar. Many theories have been proposed to account for the selective degeneration of motor neurons in ALS (for review see [17, 33]), including the involvement of autoimmune mechanisms [1], oxidative stress [28], excitotoxicity [30], and cytoskeletal abnormalities [12]. Although the cause of the disease is unknown and there is only limited understanding of the mechanisms of motor neuron loss, research data have suggested the importance of impaired calcium homeostasis in motor neuron injury. In our previous studies we found increased calcium accumulation in motor nerve terminals of sALS patients [36]. Experimentally, similar changes were induced in mice injected with immunoglobulins (IgG) isolated from sALS patients [8]. Modification of the calcium distribution within spinal motor neurons was also documented in a transgenic mouse model of familial ALS, based on the $G^{93} \rightarrow A$ mutation of the gene encoding Cu/Zn superoxide dismutase (SOD-1) [38]. Although several studies have demonstrated the importance of excitotoxic mechanism in ALS [24, 29, 30, 31], so far no data are available to show the calcium distribution at subcellular level in excitatory amino acid-induced motor neuron degeneration. In the present experiments, ultrastructural techniques were used to analyze whether changes in the calcium homeostasis are associated with excitotoxic motor neuron injury. To evoke degeneration of spinal motor neurons, rats were injected subdurally with DL-homocysteic acid (DL-HCA), an excitatory amino acid analogue of glutamate, which has been shown to induce severe lesions in motor neurons over a time scale of several hours [15]. The alterations in the distribution of intracellular calcium in the spinal motor neurons, paralleling these pathological changes, were then monitored at various survival intervals electron microscopically using the oxalate-pyroantimonate-glutaraldehyde fixation method [3, 4].

Materials and methods

In vivo excitatory amino acid application

Male, 21-day-old CFY rats were used for the experiments. Animals were anesthetized with intraperitoneal injection of a mixture of xylazine (12 mg/kg) and ketamine (108 mg/kg). An incision was made over the lower thoracic and lumbar spine, the paraspinal muscles were dissected and, to expose the lumbar spinal cord, the posterior arches of the upper lumbar vertebrae were removed over two to three segments. Following the posterior laminectomy, 730 µg DL-HCA was subdurally injected (10 µl 400 mM DL-HCA in distilled water, pH adjusted to 7.4 with NaOH). Immediately after the injection the skin was sutured and the animals were allowed to recover. Control rats were operated and injected with 10 µl distilled water (pH adjusted to 7.4) in the same way. All the experiments were performed in accordance with institutional guidelines for animal experiments and with govermental laws for animal protection (protocol no. 72/k-6/1999).

Specimen preparation and electron microscopy

Animals were allowed to survive for 1, 3, 6, or 24 h following DL-HCA injection, and then, under anesthesia, they were transcardially perfused with 3% glutaraldehyde containing

90 mM oxalic acid adjusted to pH 7.4 with KOH [3, 4]. Ten animals were used at each survival time. Spinal cords were dissected, cut into segments and fixed for additional 12 h in the same fixative. Following postfixation in 1% osmic acid containing 2% potassium pyroantimonate, spinal cord samples were dehydrated in graded series of ethanol, processed through propylene oxide and embedded in Durcupan ACM. Blocks were polymerized for 2 days at 56°C, then semithin sections with 0.5-μm nominal thickness were cut on a Sorvall MT 5000 ultramicrotome, stained according to Richardson [27] and examined under the light microscope (Olympus Vanox T) to localize large motor neurons. After trimming the blocks to the ventrolateral motor neuron pool, ultrathin (40-50 nm thick) sections were cut, mounted on formvar-coated single-hole copper grids, stained with uranyl acetate [11] and lead citrate [26] and examined in a Zeiss CEM 902 electron filtering microscope. The applied fixation procedure ensured good structural preservation and resulted in electron-dense deposits (EDDs) due to the reaction with tissue calcium. These reaction products were easily discernible under the transmission electron microscope. To guarantee the specificity of the histochemical procedure, the composition of EDDs was regularly controlled by electron spectroscopic imaging (ESI) [2] using the digital image analysis system (IBAS 2.0, Kontron) attached to the microscope. For such analysis, 20- to 30-nm unstained sections were prepared, significant calcium distribution was determined in randomly selected regions of the sections, then the calcium distribution pattern was correlated with the distribution of the EDDs. To perform the ESI analysis, individual images were recorded at 20,000-30,000 × by 80 kV accelerating voltage of the microscope, using a 90-μm objective aperture and a 650-μm spectrometer entrance aperture with a slit width of 8-10 eV. Element-specific (at the ionization edge of calcium) and background image pairs were recorded at energy loss values of 355 eV and 310 eV, respectively. Between 500 and 600 video images were recorded and averaged for each energy loss value to produce low noise images for further calculations. Next, the net calcium distribution was determined by subtracting the background image from the "edge" image. The significant calcium distribution pattern was visualized by color-coding the difference image according to the mean +2.5 SD - mean +6 SD rule. Using this method, pixels identifying a significant signal (i.e., significantly above the average) were colored and retained in the analytical image, while non-significant signals were eliminated. To check the correlation of the true calcium distribution with the pattern of the EDDs, this color-coded image was finally superimposed onto the black-and-white fine-structural digital image of the same area, recorded at the carbon absorption edge (dE=250 eV).

Results

Ultrastructural alterations and the accompanying changes of the calcium distribution of spinal motor neurons were analyzed at different time points up to 24 h following DL-HCA injection. When the animals were killed immediately after the DL-HCA application (0-h survival time), neither degenerative alterations, nor changes in the calcium distribution (Fig. 1B) compared to the untreated controls (Fig. 1A) were seen. Similarly, no ultrastructural changes were observed following subdural injection of distilled water, used as the vehicle of DL-HCA in our experiments.

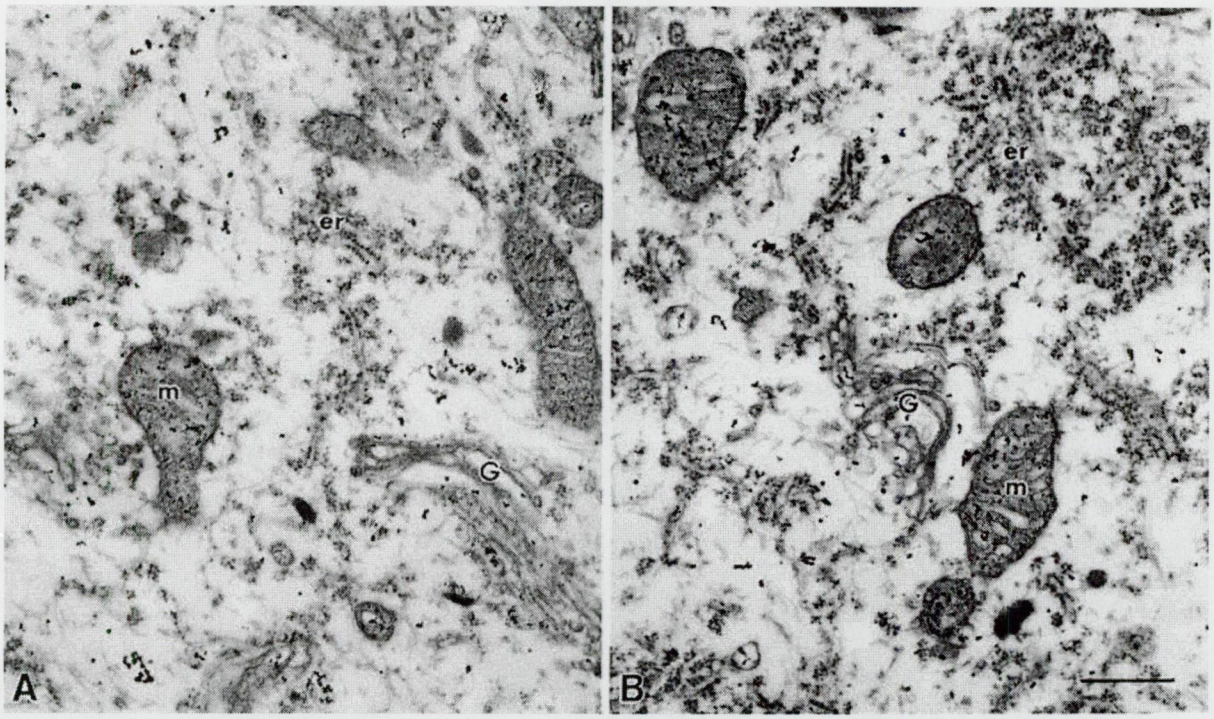

Fig. 1. A Electron micrograph of a motor neuron from the lumbar section of spinal cords of 21-day-old untreated control rats displays no structural alteration and low level of calcium. **B** At 0-h survival time the ultrastructural appearance is similar to the control, i.e., neither morphological changes nor elevated calcium are seen (*m* mitochondrion, *ER* endoplasmic reticulum, *G* Golgi apparatus). Oxalate-pyroantimonate reaction; *bar* 0.5 μm

---

By 1 h following DL-HCA injection the majority of motor neurons either showed no changes, or only cytoplasmic calcium accumulation was present (Fig. 2A). However, in a few cases initial signs of degeneration were noticed, with dilatation of cisterns of the endoplasmic reticulum (ER) and Golgi complex, paralleled with calcium accumulation. In such neurons the majority of mitochondria showed normal ultrastructure with spatially restricted calcium uptake only (Fig. 2B).

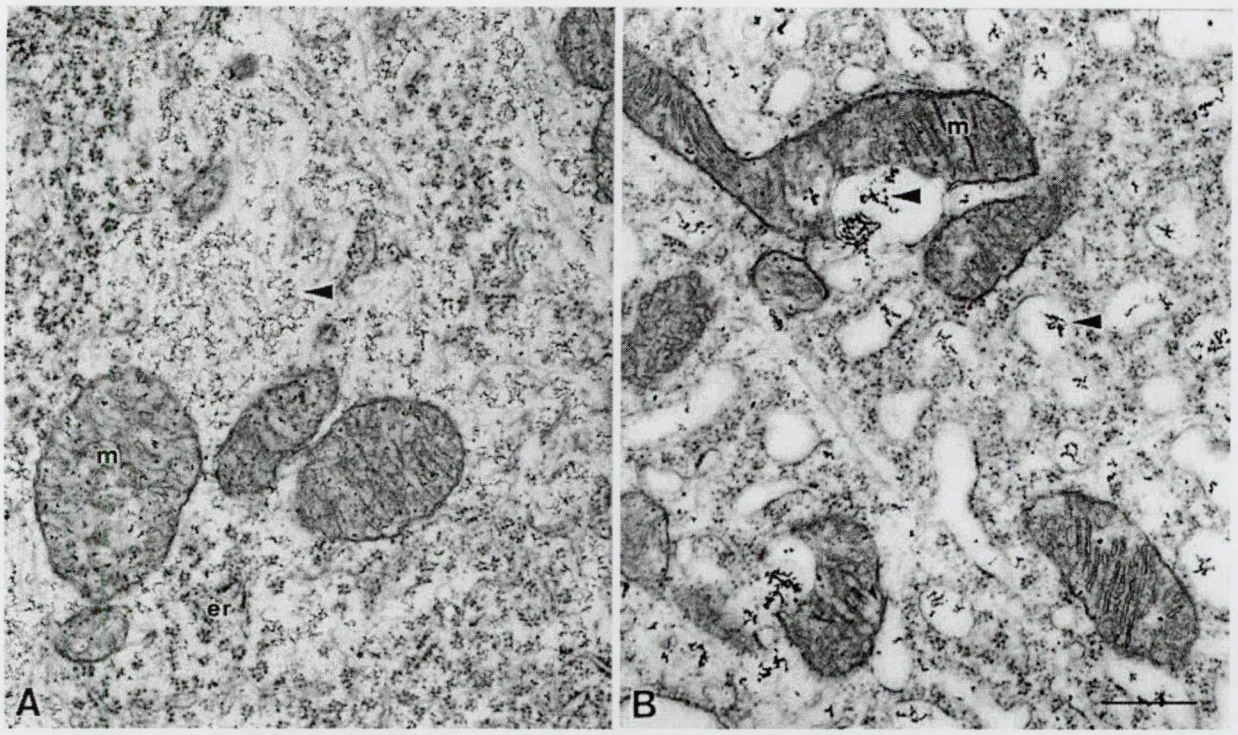

Fig. 2A, B. Electron micrographs of motor neurons from the lumbar section of the spinal cord of DL-HCA injected rats at 1-h survival time after the injection. **A** Generally, no structural alteration is seen, but regularly an elevated level of cytoplasmic calcium is present. **B** Occasionally initial signs of degeneration can be observed affecting mainly the ER, which has dilated cisterns and calcium precipitates. The majority of mitochondria are uninfluenced, with localized calcium accumulation only (DL-HCA DL-homocysteic acid, *m* mitochondrion, *arrowhead* calcium deposits). Oxalate-pyroantimonate reaction; *bar* 0.5 μm

---

Generally, a large variance of the reactions of motor neurons were noticed at each time point following DL-HCA application. This heterogeneity was most apparent after 3 h survival, when it ranged from a slight elevation of calcium paralleled with mild or no injury, to a robust calcium increase and definite degeneration. At this time point, according to their overall appearance, we arbitrarily sorted the motor neurons into three groups with signs of either (1) modest, (2) advanced or (3) profound degeneration. In the first group (modest injury) morphological changes were rarely noticed. At most, an increased calcium accumulation in the cytoplasm was documented (Fig. 3A), compared to controls (Fig. 1A), while intracellular organelles did not show elevated levels of calcium. In the second group (advanced lesion) morphological changes were significant in the majority of motor neurons. Although all the cytoplasmic organelles were affected in some way, large variations were observed with regards to the distinct features of the degeneration and the actual distribution of intracellular calcium. In some of the neurons the degeneration involved mainly the ER and the Golgi apparatus in such a way that they exhibited an increased calcium content (Fig. 3B), while the neighboring mitochondria displayed calcium content comparable to controls (cf. Fig. 1A, Fig. 3B). In some other motor neurons, a contrasting picture could be seen: mitochondrial calcium accumulation and partial swelling (Fig. 3C) was paralleled by the depletion of calcium from the adjacent organelles. Finally, a rather homogeneous calcium uptake was also observed, with elevated calcium level in both swollen mitochondria and dilated cisterns of the nearby structures. In the third group (profound degeneration), the cytoplasm of motor neurons

regularly contained vacuoles of different sizes (Fig. 3D), which were identified as dilated fragments of the Golgi apparatus or cistern of the ER system. In most of the cases, but not always, these vacuoles contained clusters of calcium precipitates. Unlike these organelles, all the perikaryonal mitochondria appeared dark and shrunken, with significantly decreased or absent calcium content.

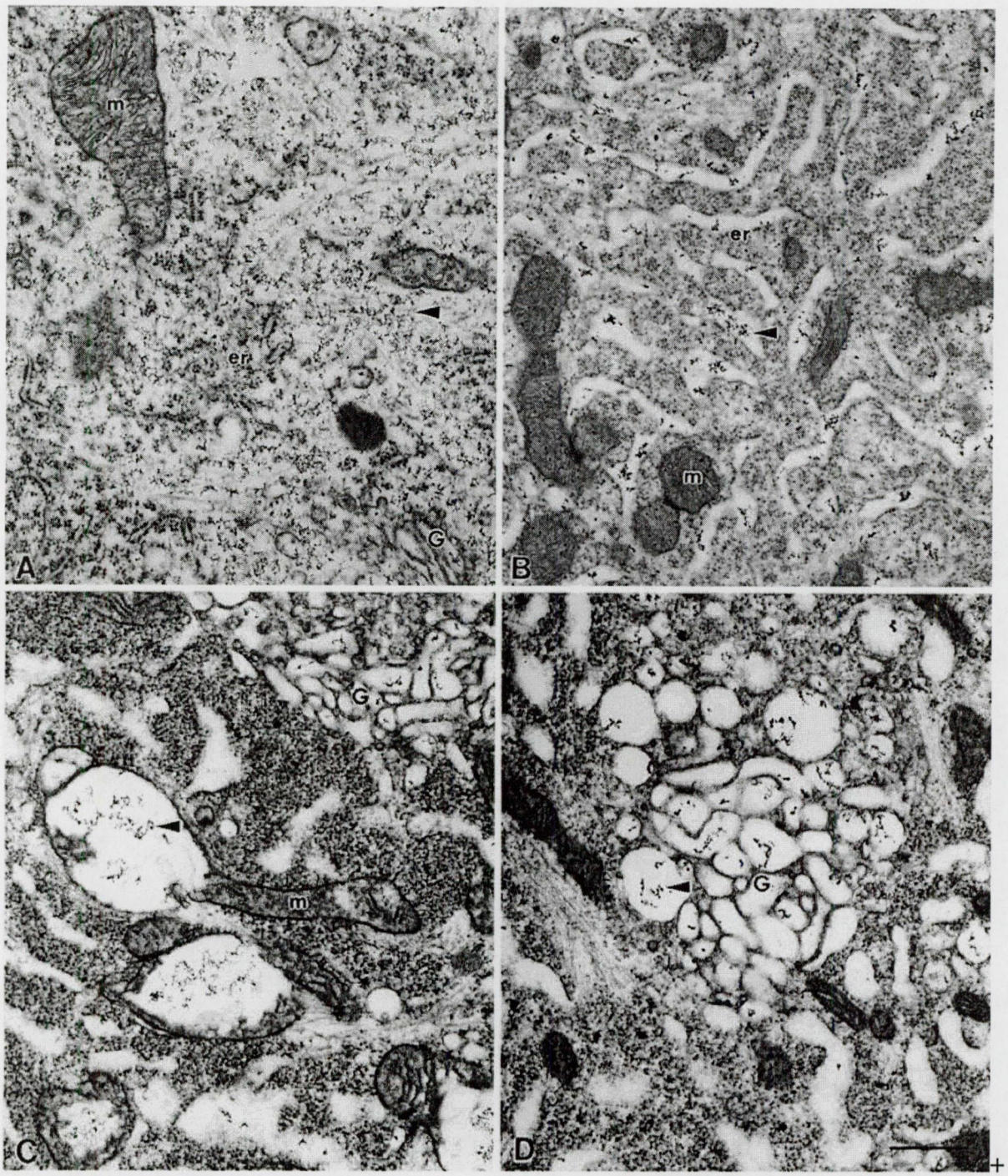

Fig. 3A-D. Electron micrographs of spinal motor neurons from a DL-HCA-injected rat in different stages of degeneration 3 h following injection. **A** Early phase of degeneration (modest stage). While the structural integrity of motor neurons is not changed, a cytoplasmic calcium increase can be detected. **B** Advanced degeneration. Cisterns of the ER are dilated and contain calcium deposits. Mitochondria are somewhat compressed, likely due to the

osmotic pressure originating from the dilatation of the neighboring organelles; however, their membrane structure is intact; furthermore, they contain EDDs comparable to the control only (Fig. 1A). **C** Advanced degeneration. Localized mitochondrial swelling and calcium accumulation is seen, while the neighboring swollen ER and Golgi complex contain no, or minimal amount of calcium. **D** Profound degeneration. At this stage of degeneration an advanced vacuolization is seen. The vacuoles may originate from the ER or from the fragmented Golgi system. In most of the cases these vacuoles contain clusters of precipitates, while the shrunken and dark mitochondria are regularly devoid of calcium (*EDDs* electron-dense deposits, *m* mitochondrion, *ER* endoplasmic reticulum, *G* Golgi apparatus, *arrowhead* calcium deposits). Oxalate-pyroantimonate reaction; *bar* 0.5 μm

---

At 6 h after the injection, strong fragmentation and vacuolization of both the endoplasmic reticulum system and the Golgi apparatus was documented (Fig. 4A). Various-sized clusters of calcium precipitates were regularly present in the enlarged, swollen cisternae of the organelles. At this survival time mitochondria were typically dark and shrunken, with no visible EDDs inside. Generally, the ultrastructure and the calcium distribution of these neurons was similar to those in the third group (profound degeneration) of the 3-h material (Fig. 3D).

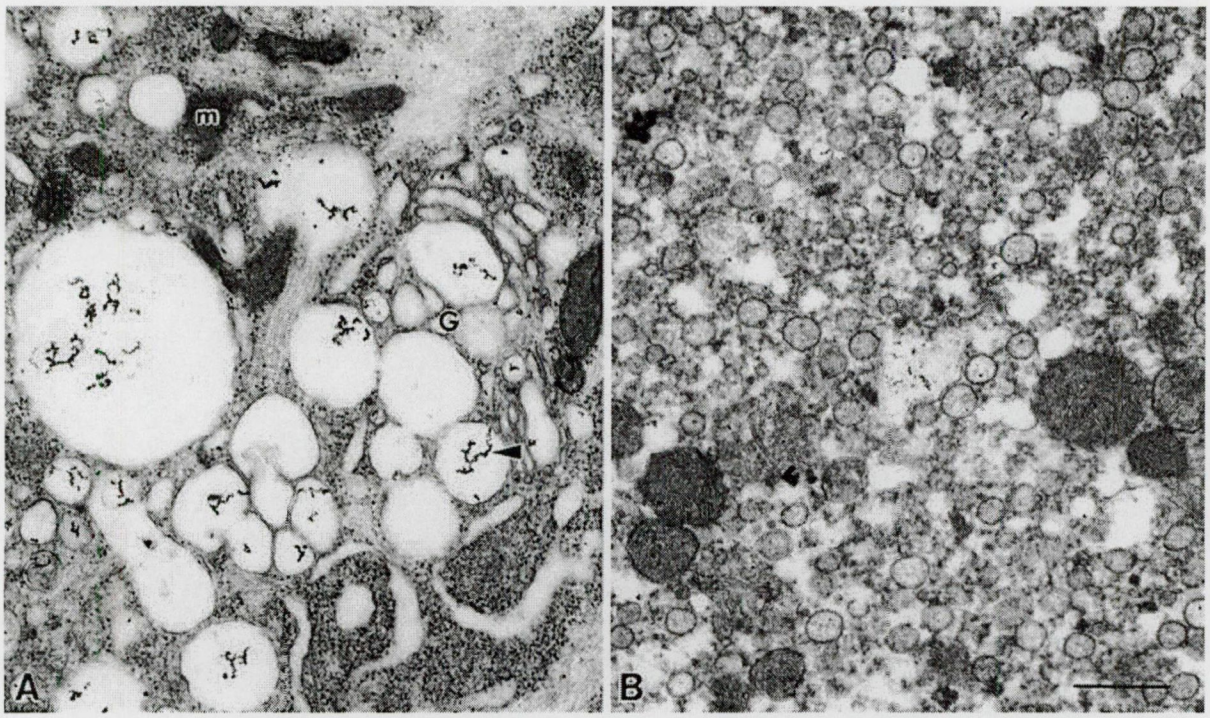

Fig. 4A, B. Electron micrographs of motor neurons from the lumbar section of the spinal cord of DL-HCA-injected rats at 6- and 24-h survival times after the injection. **A** At 6 h survival time profound structural alterations are seen with advanced vacuolization of the Golgi complex and the ER, paralleled by calcium accumulation, while the mitochondria are regularly shrunken and dark with no visible calcium. **B** At 24 h following DL-HCA injection a total disintegration of the cytoplasmic structure is seen, and most of the organelles are degenerated beyond recognition (*m* mitochondrion, *G* Golgi apparatus, *arrowhead* calcium deposits). Oxalate-pyroantimonate reaction; *bar* 0.5 μm

By 24 h following DL-HCA injection most of the motor neurons had lost their structural integrity and only few of the cytoplasmic organelles remained recognizable (Fig. 4B). Nearly all of the organelles had lost their normal conformation, and were fragmented and degenerated beyond recognition. Very low calcium level was only seen within the neurons at this stage of degeneration.

An interesting aspect of the present results is the recognition that, at least in this excitotoxicity model, mitochondria are able to exert a non-homogeneous volumetric response to the environmental stress when either the mitochondrial swelling or the mitochondrial calcium uptake is considered. We detected mitochondria with local swelling and increased calcium in this small swollen volume fraction, affecting only a very small proportion of the actual mitochondrial volume (Fig. 5A, B). In addition, mitochondria in which swelling and calcium uptake extended to a dominant proportion of the mitochondrial volume were observed. However, in these mitochondria the remaining volume fraction showed normal ultrastructure and low level of calcium (Fig. 5C, D). Finally, mitochondria were also observed with increased calcium distributed homogeneously in the swollen mitochondrial volume (Fig. 5E, F).

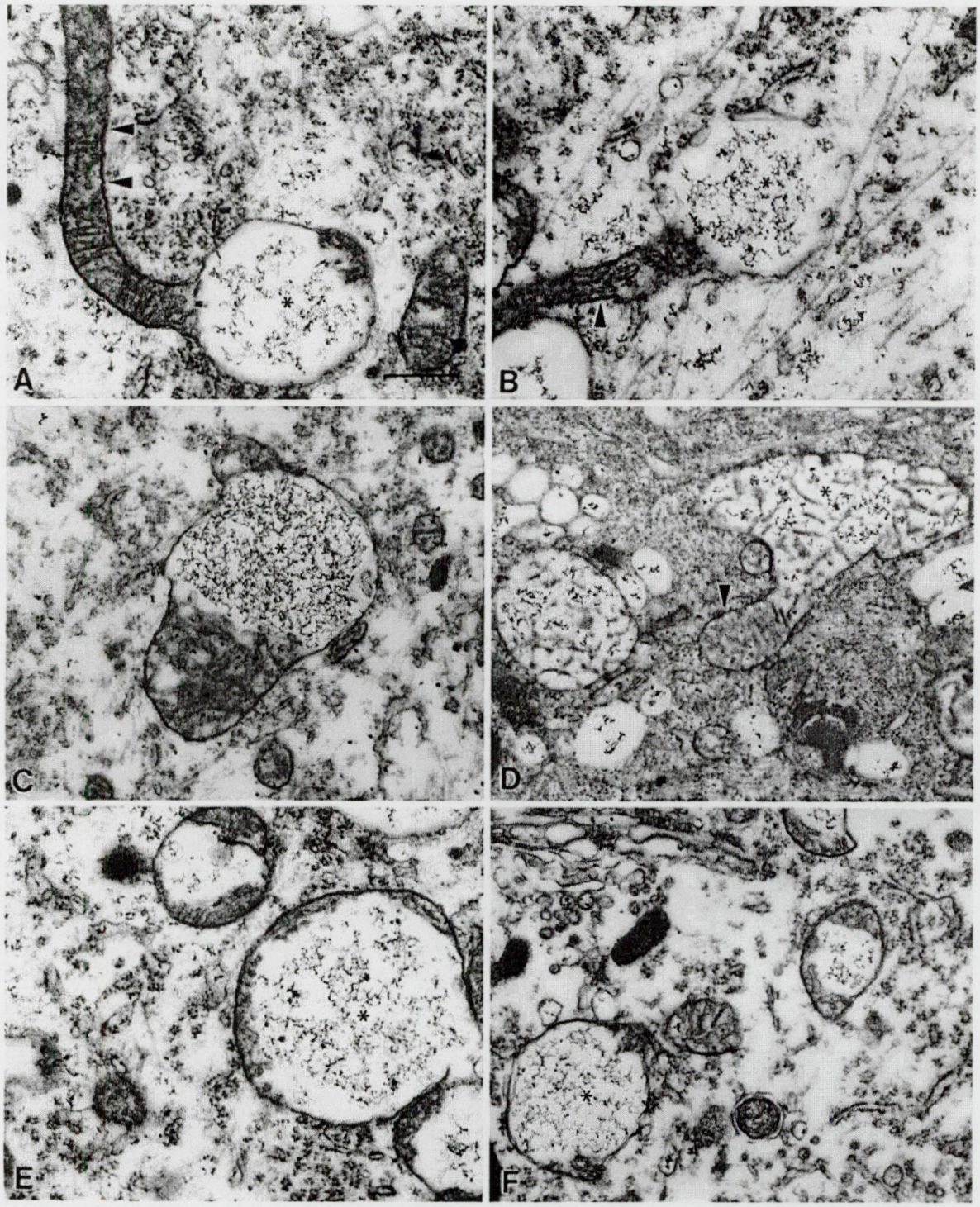

Fig. 5A-F. Electron micrographs of mitochondria in different stages of degeneration with various amounts of calcium. **A**, **B** According to the proposed sequence of alterations, during the first phase the structural disintegration and the calcium accumulation are local (*asterisks*); the majority of the mitochondrial volume has a normal structure (*arrowheads*). **C**, **D** Next, a more advanced swelling, paralleled by an increased calcium accumulation can develop (*asterisks*), which results in a marked decrease of intact mitochondrial volume (*arrowhead* in **C**). **E**, **F** Finally, mitochondria reach a state with extensive swelling and ample calcium uptake (*asterisks*). It is suggested that mitochondrial swelling does not take places uniformly throughout the mitochondria, but propagates along a direction within the mitochondria; furthermore, since the electron microscopy technique could capture these differently evolved

conditions, it is likely that they can exist for a prolonged time. Oxalate-pyroantimonate reaction; *bar* 0.5 μm

Discussion

In the present experiments DL-HCA, an excitotoxic analogue of glutamate that interacts with both NMDA and non-NMDA receptor subtypes, was used to trigger the degeneration of motor neurons. DL-HCA was effective in inducing a robust injury of spinal motor neurons and, unlike kainate or AMPA [15], was well tolerated by the animals during the 24-h survival period. Spasms of the tail and hindlimbs were seen for 1-2 min immediately after the subdural injection of DL-HCA, likely due to a strong hyperactivation of lumbar motor neurons, but no further clinical sign of the effect of the excitotoxin was noted during the whole observed period. Several attempts have been made to optimize the dose and the method of application of DL-HCA. First, direct drainage of DL-HCA to the exposed spinal cord was tested, after removing the dura [15], and then different concentrations/dosages of the compound were examined. However, reproducible results were obtained only using subdural injection, and only at a dose not smaller than 700 μg DL-HCA. Furthermore, no immediate reactions of the animals were noticed, suggesting hyperexcitation, when lower doses of the drug were injected. In control rats, injected with distilled water alone, neither clinical signs of motor dysfunction, nor pathological/ultrastructural alteration of motor neurons were observed. Since the ultrastructural pathology of the spinal cord after a similar acute and invasive application of DL-HCA has already been extensively described [15], we confined our study to following the alterations of motor neurons and to determining the concurrent changes in their intracellular calcium distribution.

The credibility of our results, describing the modification of the intracellular calcium distribution during degeneration of motor neurons following an excitotoxic insult, depends fundamentally on the histochemical fixation. The oxalate-pyroantimonate preparation procedure, to fix and visualize the subcellular distribution of calcium, provides good ultrastructural preservation and does not induce structural alterations, as we described earlier [37]. Furthermore, the specificity of the histochemical reaction for calcium has already been confirmed with energy dispersive X-ray microanalysis [5], and electron spectroscopic imaging [6, 8, 9, 35, 36]. Finally, the procedure proved to be applicable to following function-dependent changes of neuronal calcium distribution not only in our hands [38], but also in other laboratories [21, 25]. Nevertheless, the calcium content of the EDDs was regularly checked and verified during the present study using the ESI method [2] (Fig. 6a, b).

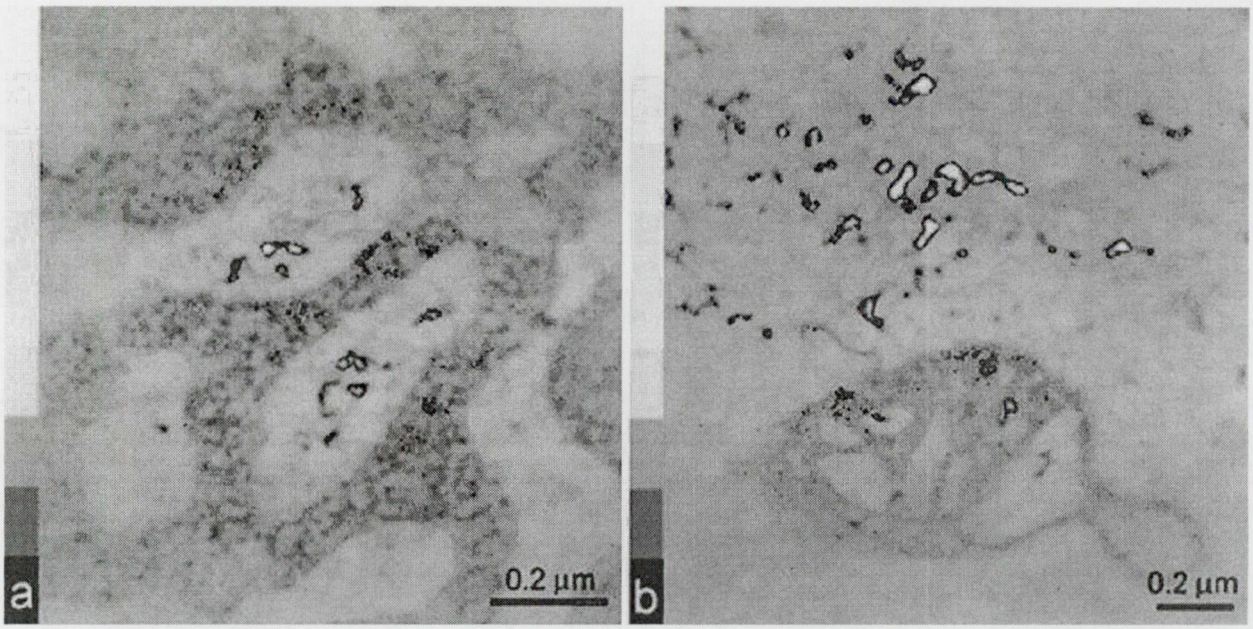

Fig. 6a, b. Analytical proof of the calcium content of the electron-dense precipitates obtained with the oxalate-pyroantimonate procedure. Calcium distribution was determined by the electron spectroscopic imaging method and exemplified in two randomly selected fields. **a** Dilated cisterns of the ER with internal calcium precipitates; **b** partially swollen mitochondrion surrounded by scattered cytoplasmic calcium deposits. The significant calcium signal was color coded according to the actual significance value at each pixel above the 2.5 SD significance level (*red*) up to the 6.0 SD value (*white*). The true (*colored*) calcium signal can be adequately correlated with the EDDs

---

We noticed a great diversity in the reaction of motor neurons after subdural injection of DL-HCA when the ultrastructural alterations or the calcium distribution were observed. Besides the biological variations, this heterogeneity might be largely attributed to methodological problems, such as unintended, slight, but nonreproducible physical injury of the spinal cord during the removal of the posterior arches of the vertebrae, or uneven diffusion of the DL-HCA into the tissue. However, the time course analysis helped to reconstruct the conceivable sequence of the alteration of the ultrastructure and calcium distribution from the initial step of the degeneration until the cell death. In the earliest stage, neither calcium accumulation, nor ultrastructural changes were seen (Fig. 1B). Later, when structural alterations still could not be noticed, elevated calcium levels were detected in the cytoplasm of motor neurons, while the organelles were unaffected, having calcium content comparable to the controls (Figs. 2A, 3A). Next, a redistribution of the intracellular calcium from the cytoplasm to membrane-enclosed organelles started, mainly to the ER and mitochondria (Figs. 2B; 3B, C), which was accompanied by a gradual conformational change of these structures (dilatation of the cisternae, fragmentation). Before the final disintegration and elimination of the calcium content of the cells (Fig. 4B), a progressive degeneration of the organelles was seen (Figs. 2, 3). At this stage, the gravity point of the calcium distribution could be set either to mitochondria, or to the ER/Golgi apparatus, or to both. Nevertheless, accepting that at the time of fixation individual neurons might be at differently advanced stages in the course of degeneration, this scenario could be brought in accord with the cooperative role of the ER and mitochondria in handling of intracellular calcium [*13*].

As the appropriate surface receptors are activated, calcium influx and release from the internal stores (due to the activation of the inositol triphosphate receptors of the ER) could lead to an increase of the intracellular calcium [*34*]. Consecutively, mitochondrial calcium uptake takes place, even under physiological conditions [*39*], preferably at those microdomains where the ER and mitochondria are at intimate proximity (see Fig. 2B) [*22*]. If the calcium load is high enough, however, a biphasic mitochondrial calcium uptake can be induced, at least in vitro [*13*], before the final collapse of the mitochondrial homeostasis occurs. In the first phase, this uptake is not paralleled by detectable mitochondrial swelling [*13*], which might correspond to those mitochondria in our material where only local calcium accumulation could be seen (Figs. 2B; 5A, B). The second phase, accompanied by gradual swelling of the organelles (Figs. 3C; 5C-F) could eventually lead to opening of mitochondrial permeability transition pore in its high conductance state, release of matrix calcium and disintegration of the organelles (Figs. 3D, 4A). Although an ATP-dependent reload of the ER stores could take place parallel to these mitochondrial events (Fig. 3B), the collapse of mitochondrial ATP synthesis should also induce a secondary depletion of such stores. Finally, the mitochondrial permeability transition leads to the release of apoptosis-inducing factors, which results in apoptotic or necrotic cell death, depending on the available energy (ATP) of the actual cell [*18*, *23*] (Fig. 4B). Our results indicate that a cytoplasmic calcium increase followed by a relocation of calcium to mitochondria are essential steps leading to excitotoxic motor neuronal death. These findings are also supported by in vitro experiments, in which a similar sequence of changes in the intracellular calcium were documented, irrespective of whether apoptotic or necrotic type of cell death was induced [*19*].

Our present study has been aimed at analyzing the role of calcium in a model of ALS, a prototype of motor neuron diseases. During previous investigations of human biopsy material using electron microscopic histochemistry we documented an elevated level of mitochondrial and vesicular calcium in motor nerve terminals from biceps muscles of sALS patients [*36*]. These findings were corroborated in subsequent experiments employing the passive transfer model of sALS, by demonstrating a calcium increase not only in motor axon terminals of the interosseus muscle, but also in the cell bodies of spinal motor neurons [*8*]. The most authentic models for fALS are based on transgenic animals carrying the same mutations of the SOD-1 gene taht were detected in a subpopulation of the ALS patients [*10*]. Applying the calcium histochemistry technique to this model, we also documented a gradual elevation of intracellular calcium in spinal, but not in parvalbumin-rich oculomotor neurons, which was paralleled by their different degeneration [*38*]. As an extension of these studies, in the present experiments we showed an increased level of calcium in spinal motor neurons after application of a glutamate analogue, suggesting an important role of the impairment of the calcium homeostasis during excitotoxicity (another well-accepted model of sALS [*16*]). Assuming that ALS may be a multifactorial disease [*7*], on the basis of the above results, we suggest that alteration in the intracellular calcium level and/or distribution might be the crucial element in its pathomechanism. Appropriate changes in the subcellular calcium concentration could result in the proliferation and synchronization of a variety of distress conditions and, irrespective of the actual initiating element, could lead to a uniform clinical picture of the disease. Indeed, data are already available indicating a calcium-dependent interplay of the excitotoxic injury and the degeneration of motor neurons induced by the mutant SOD-1 enzyme [*32*]. Furthermore, an increased glutamate level in the cerebrospinal fluid of rats was demonstrated in the passive transfer model of sALS [*20*], suggesting an interaction of immune-mediated and excitotoxic processes. Further studies aimed at experimentally influencing the stability of motor neuronal calcium homeostasis, e.g., through

the regulation of certain calcium binding proteins, like parvalbumin or calbindin D-28K, may help to prove the pivotal role of calcium ions in the pathomechanism of ALS.

Acknowledgements. This work was supported by the National Scientific Research Fund of Hungary (OTKA T 026239, T 034314, M 36252), the Hungarian Ministry of Welfare (ETT T04/001/2000, T05/028/2000), the Hungarian Ministry of Higher Education (FKFP 0032/2000) and the US-Hungary Science and Technology Fund (JF-661).

References

1.Appel SH, Alexianu ME, Engelhardt JI, Siklós L, Smith RG, Mosier D, Mohamed H (2000) Involvement of immune factors in motor neuron cell injury in amyotrophic lateral sclerosis. In: Brown RH Jr, Meininger V, Swash M (eds) Amyotrophic lateral sclerosis. Martin Dunitz, London, pp 309-326

2.Bauer R (1988) Electron spectroscopic imaging: an advanced technique for imaging and analysis in transmission electron microscopy. Methods Microbiol 20:113-146

3.Borgers M, De Brabander DM, Van Reempts DJ, Awouters F, Jacob WA (1977) Intranuclear microtubules in lung mast cells of guinea pigs in anaphilactic shock. Lab Invest 37:1-8

4.Borgers M, Thoné EF, Van Neuten JM (1981) The subcellular distribution of calcium and effects of calcium antagonists as evaluated with a combined oxalate-pyroantimonate technique. Acta Histochem S24:327-332

5.Dux E, Kloiber O, Hossmann KA, Siklós L (1987) Calcium in hippocampus following lidocaine-induced seizures: an electron cytochemical study. Acta Biol Hung 38:213-224

6.Dux E, Oschiles U, Uto A, Kusumoto M, Siklós L, Joó F, Hossmann KA (1996) Serum prevents glutamate-induced mitochondrial calcium accumulation in primary neuronal cultures. Acta Neuropathol 92:264-272

7.Eisen A (1995) Amyotrophic lateral sclerosis is a multifactorial disease. Muscle Nerve 18:741-752

8.Engelhardt JI, Siklós L, Kömüves L, Smith RG, Appel SH (1995) Passive transfer of amyotrophic lateral sclerosis (ALS) immunoglobulin to mice selectively increases intracellular calcium and induces ultrastructural changes in motor neurons. Synapse 20:185-199

9.Engelhardt JI, Siklós L, Appel SH (1997) Altered calcium homeostasis and ultrastructure in motor neurons of mice caused by passively transferred anti-motoneuronal IgG. J Neuropathol Exp Neurol 56:21-39

10.Gurney ME (2000) Transgenic animal models of amyotrophic lateral sclerosis. In: Brown RH Jr, Meininger V, Swash M (eds) Amyotrophic lateral sclerosis. Martin Dunitz, London, pp 251-262

11.Hayat MA (1970) Principles and techniques of electron microscopy, vol 1. Biological applications. Van Nostrand Reinhold, New York, pp 264-274

12.Hirano A (1991) Cytopathology of amyotrophic lateral sclerosis. Adv Neurol 56:91-101

13.Ichas F, Mazat JP (1998) From calcium signaling to cell death: two conformations for the mitochondrial permeability transition pore. Switching from low to high conductance state. Biochim Biophys Acta 1366:33-50

14.Ince P (2000) Neuropathology. In: Brown RH Jr, Meininger V, Swash M (eds) Amyotrophic lateral sclerosis. Martin Dunitz, London, pp 83-112

15.Ikonomidou C, Qin QY, Labruyere J, Olney JW (1996) Motor neuron degeneration induced by excitotoxins agonists has features in common with those seen in the SOD-1 transgenic mouse model of amyotrophic lateral sclerosis. J Neuropathol Exp Neurol 55:211-224

16.Jackson M, Rothstein JD (2000) Excitotoxicity in amyotrophic lateral sclerosis. In: Brown RH Jr, Meininger V, Swash M (eds) Amyotrophic lateral sclerosis. Martin Dunitz, London, pp 263-278

17.Julien JP (2001) Amyotrophic lateral sclerosis: unfolding the toxicity of the misfolded. Cell 104:581-591

18.Kroemer G, Dallapporta B, Resche-Rigon M (1998) The mitochondrial death/life regulator in apoptosis and necrosis. Annu Rev Physiol 60:619-642

19.Kruman II, Mattson MP (1999) Pivotal role of mitochondrial calcium uptake in neural cell apoptosis and necrosis. J Neurochem 72:529-540

20.LaBella V, Goodman JC, Appel SH (1997) Increased CSF glutamate following injection of ALS immunoglobulins. Neurology 48:1270-1272

21.Mata M, Staple J, Fink DJ (1986) Changes in intra-axonal calcium distribution following nerve crush. J Neurobiol 17: 449-467

22.Mattson MP, LaFerla FM, Chan SL, Leissring MA, Shepel PN, Geiger JD (2000) Calcium signaling in the ER: its role in neuronal plasticity and neurodegenerative disorders Trends Neurosci 23:222-229

23.Nicotera P, Lipton SA (1999) Excitotoxins in neuronal apoptosis and necrosis. J Cereb Blood Flow Metab 19:583-591

24.Plaitakis A (1991) Altered glutamatergic mechanisms and selective motor neuron degeneration in amyotrophic lateral sclerosis: possible role of glycine. Adv Neurol 56:319-326

25.Pullen AH, Humphreys P (2000) Ultrastructural analysis of spinal motor neurons from mice treated with IgG from ALS patients, healthy individuals, or disease controls. J Neurol Sci 180:35-45

26.Reynolds ES (1963) The use of lead citrate at high pH as an electron-opaque stain in electron microscopy. J Cell Biol 17:208-212

27.Richardson KC, Jarett L, Finke EH (1960) Embedding in epoxy resins for ultrathin sectioning in electron microscopy. Stain Technol 35:313-323

28.Rosen DR, Siddique T, Patterson D, et al (1993) Mutation in Cu/Zn superoxide dismutase are associated with familial amyotrophic lateral sclerosis. Nature 362:59-62

29.Rothstein JD, Martin LJ, Kuncl RW(1992) Decreased glutamate transport by the brain and spinal cord in amyotrophic lateral sclerosis. N Engl J Med 326:1464-1468

30.Rothstein JD, Van Kammen M, Levey AI, Martin LJ, Kuncl RW (1995) Selective loss of glial glutamate transporter GLT-1 in amyotrophic lateral sclerosis. Ann Neurol 38:73-84

31.Rothstein JD, Dykes-Hoberg M, Pardo CA, Bristol LA, Jin L, Kuncl RW, Kanai Y, Hediger MA, Wang Y, Schielke JP, Welty DF (1996) Knock-out of glutamate transporters reveals a major role for astroglial transport in excitotoxicity and clearance of glutamate. Neuron 16:675-686

32.Roy J, Minotti S, Dong L, Figlewicz DA, Durham HD (1998) Glutamate potentiates the toxicity of mutant Cu/Zn-superoxide dismutase in motor neurons by postsynaptic calcium-dependent mechanisms. J Neurosci 18:9673-9684

33.Shaw PJ, Eggett CJ (2000) Molecular factors underlying selective vulnerability of motor neurons to neurodegeneration in amyotrophic lateral sclerosis. J Neurol 247 [suppl 1]:17-27

34.Siesjö BK, Hu B, Kristián T (1999) Is the cell death pathway triggered by the mitochondrion or the endoplasmic reticulum? J Cereb Blood Flow Metab 19:19-26

35.Siklós L, Kuhnt U (1994) Calcium accumulation by dendritic mitochondria declines along the apical dendrites of pyramidal neurons in area CA1 of guinea pig hippocampal slices. Neurosci Lett 173:131-134

36.Siklós L, Engelhardt J, Harati Y, Smith RG, Joó F, Appel SH (1996) Ultrastructural evidence for altered calcium in motor nerve terminals in amyotrophic lateral sclerosis. Ann Neurol 39:203-216

37.Siklós L, Kuhnt U, Párducz Á, Szerdahelyi P (1997) Intracellular calcium redistribution accompanies changes in total tissue Na^+, K^+, and water during the first two hours of in vitro incubation of hippocampal slices. Neuroscience 79:1013-1022

38.Siklós L, Engelhardt JI, Alexianu ME, Gurney ME, Siddique T, Appel SH (1998) Intracellular calcium parallels motor neuron degeneration in SOD-1 mutant mice. J Neuropathol Exp Neurol 57:571-587

39.Werth JL, Thayer SA (1994) Mitochondria buffer physiological calcium loads in cultured rat dorsal root ganglion neurons. J Neurosci 14:348-356